50 Copies

NATIONAL AERONAUTICS AND SPACE ADMINISTRATION

Technical Report 32-1271

Plasma Characteristics of the Electron Bombardment Ion Engine

T. D. Masek

JET PROPULSION LABORATORY

CALIFORNIA INSTITUTE OF TECHNOLOGY

PASADENA, CALIFORNIA

April 15, 1968

NATIONAL AERONAUTICS AND SPACE ADMINISTRATION

Technical Report 32-1271

Plasma Characteristics of the Electron Bombardment Ion Engine

T. D. Masek

Approved by:

D. R. Bartz, Manager
Research and Advanced
Concepts Section

JET PROPULSION LABORATORY
CALIFORNIA INSTITUTE OF TECHNOLOGY
PASADENA, CALIFORNIA

April 15, 1968

JPL TECHNICAL REPORT 32-1271

Prepared Under Contract No. NAS 7-100
National Aeronautics & Space Administration

Contents

Figures

Figures (contd)

Abstract

An analytical study is presented as a first step in developing a model for engine operation. Solutions for the plasma potential distribution and the ion beam current are derived in terms of the electron and ion temperatures and densities. Experimental data, obtained with a Langmuir probe in mercury and cesium engines, are used to determine coefficients required in the plasma potential solutions. The use of these coefficients in the ion beam solution produced results consistent with Faraday probe measurements of the beam current.

Plasma Characteristics of the Electron Bombardment Ion Engine

I. Introduction

Continuing interest in the application of the electron bombardment ion engine to future spacecraft has prompted studies of the overall operation of such engines (Refs. 1–3). These studies have concentrated primarily on ion extraction, ion focusing, and on general performance characteristics; they have been, in general, quite successful. Engines of this type have operated for many thousands of hours with both mercury and cesium as propellants. However, the plasma which is the source of ions for the engine has not been examined extensively. Previous investigations (Refs. 4–6) have presented experimental data on the plasma properties and have analyzed these properties; thus far, however, a general analytical model predicting the plasma characteristics is not available.

The need for an analytical model is clear considering that most improvements and optimizations of the electron bombardment engine have been based on experimental trial and error methods. Since the formation of the plasma represents the major source of engine inefficiency, information on the formation mechanisms and the factors affecting plasma properties would be useful in the design of new engines and improvement of existing ones. Specifically, factors such as propellant distribution, cathode position, and engine geometry, which are presently studied only experimentally, could be analytically assessed more generally. In addition, it would be useful to determine scaling relationships to simplify future engine development. Basic solutions for the plasma properties and scaling factors can be determined only after a model is developed. The purpose of this report is to develop an analytical model for the plasma and to indicate the steps and assumptions involved in obtaining solutions.

The equations describing the plasma are nonlinear partial differential equations requiring numerical solutions in general. However, by making certain reasonable assumptions, the equations of motion for ions and electrons can be simplified to allow a solution for the radial and axial plasma potential in terms of the ion density. The ion density cannot be solved for analytically because the flux continuity equations include a nonlinear ion production term; however, the plasma potential solutions can be applied and compared to measure potentials by using measured ion densities in the solutions. In addition, by using the plasma potential solutions, the axial ion flux

density can be obtained and compared with measured ion flux in the beam to provide an additional correlation of theory and measurement. This procedure provides a method for justifying the assumptions and determining the validity of the analytical model. The results of this study provide a starting point for the complete solution of the plasma equations.

II. Plasma Theory

A typical electron bombardment ion engine is shown schematically in Fig. 1. The engine is composed of the following elements: cathode, anode, housing, magnetic field coil, screen grid, and accelerating grid. The cathode thermionically provides electrons, which are attracted toward the anode. The axial magnetic field produced by the field coil causes the electrons to have spiral paths and increases their effective mean free path. Propellant gas injected into the chamber is ionized by the electrons to form a plasma of ions, electrons, and neutral atoms. In the ensuing discussion, two groups of electrons will be identified: primary and Maxwellian electrons. Primary electrons, those initially emitted from the cathode, have energies approximately equal to the cathode–anode potential difference (Ref. 7) and form an essentially monoenergetic group. Collisions of primary electrons with neutral atoms produce ions and secondary electrons. The primary electrons lose energy through inelastic collisions with atoms, ions, and secondary electrons. A portion of the primary group thus joins the lower-energy secondary group, which is found to have a Maxwellian energy distribution. One could reasonably expect a radially decreasing average Maxwellian energy due to the decreasing energy contribution of the primary group.

The plasma thus formed is a source of ions. A sheath formed at the screen grid provides a boundary for the plasma. Ions crossing this sheath and passing through the holes in the grid are accelerated by the electric field applied between the grids. In addition to the plasma ion loss by extraction in the beam, ions are lost through recombination in the plasma, at the cathode, and on other engine chamber surfaces.

Engine operation and efficiency are thus strong functions of the efficiency of ion production, ion loss, and the

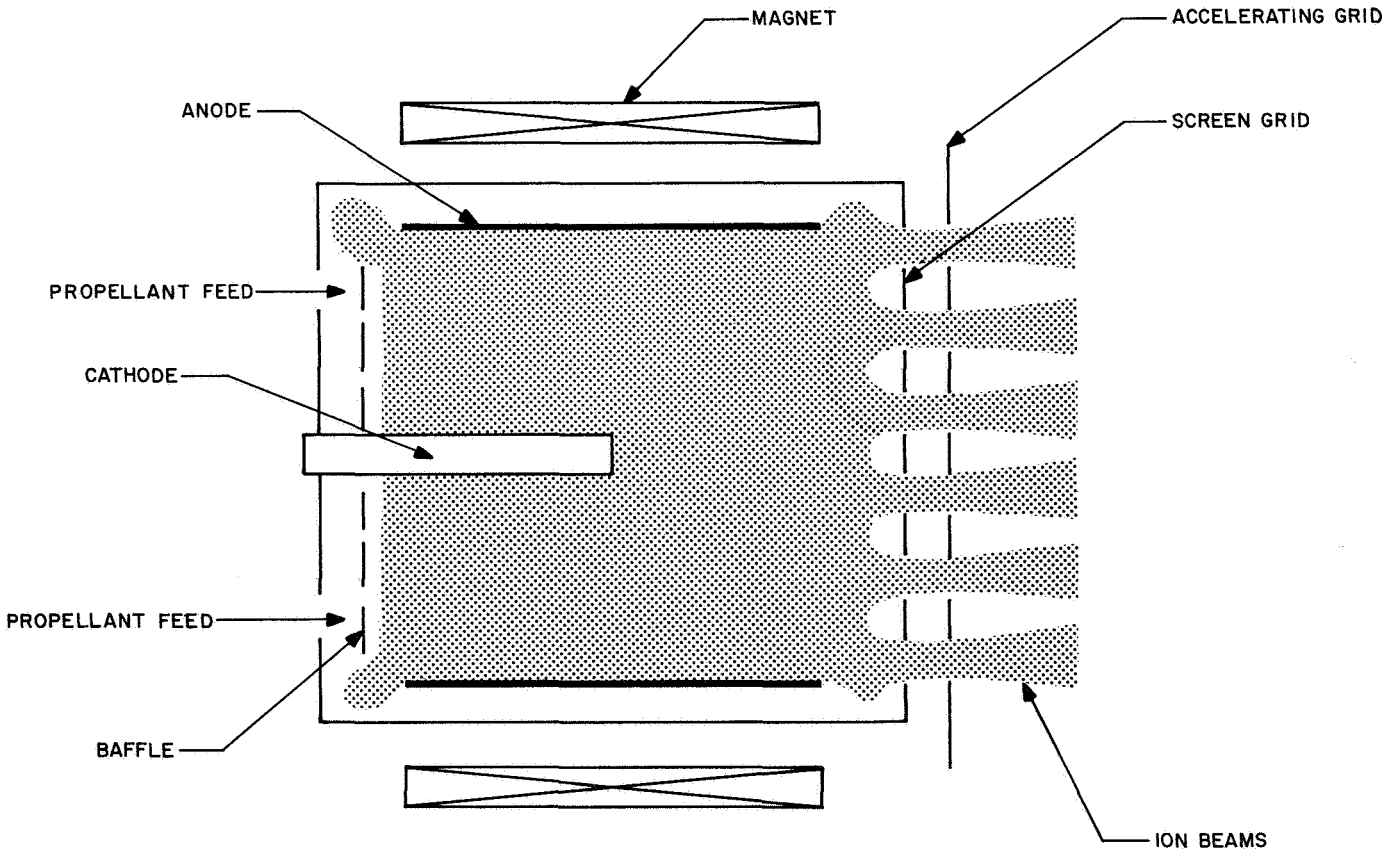

Fig. 1. Conventional electron bombardment ion engine

axial motion of the ions at the screen grid. Ion production, loss, and axial motion are dependent upon the properties of the plasma. That is, they depend on the ion density, electron energy, and plasma potential distributions. Therefore, the analysis must deal with these properties.

An analytical model of the plasma as it relates to the electron bombardment ion engine will be developed here. It is important to realize that the results of this study relate directly to the bombardment engine through the assumptions and the application of experimental data. The assumptions should be reviewed before application is made to other situations.

As noted, the plasma can be completely described by a series of nonlinear, partial differential equations. To obtain useful information from these equations requires a number of simplifying assumptions. A large body of literature exists in which the effects of various assumptions on the solutions are investigated. However, the choice of assumptions for any given application must be based on the properties of the particular plasma being studied. First, therefore, the general characteristics of the plasma will be presented in terms of collision times, collision and ionization cross sections, and ion production coefficients. These will be used to justify the assumptions made in the analysis that follows. Second, the general equations describing the plasma are presented, and the assumptions to be made in the solution are discussed. An analytical solution for the plasma potential is obtained, and compared with experimental data to check the validity of the analysis. The solution will be used in later work to find numerical solutions to the flux continuity equations for the ion density. Finally, the equation for the axial ion flux is derived and put in terms of the ion density gradient. This flux is computed and compared to measured beam current densities. An energy equation for the primary and Maxwellian electrons has not yet been established, but this does not limit the analysis presented here.

A. General Characteristics

As indicated previously, the primary electrons enter the plasma with energies approximately equal to the arc (cathode–anode) voltage. Collisions of primary electrons with secondary electrons and neutrals reduce a portion of the primary electrons to a Maxwellian distribution. The time required for primary electron energy to be lost can be estimated by considering collision and relaxation times.

In steady state, the time required for a monoenergetic distribution of primary electrons of energy ϵ_p to relax to a Maxwellian distribution with energy $(3/2)\,kT_e$ when interacting with a Maxwellian group of this same energy is given approximately by (Ref. 8)

$$\tau_e = \frac{3.20 \times 10^4\, \epsilon_p^{3/2}}{n_e\, G(\xi) \ln \Lambda} \tag{1}$$

where

ϵ_p = primary electron energy, eV

T_e = electron temperature, °K

n_e = electron number density, m^{-3}

$\ln \Lambda = \ln \left[12\pi\, (\epsilon_0\, kT_e)^{3/2}/e^3\, n_e^{1/2}\right]$

with

k = Boltzmann constant, J/°K^{-1}

ϵ_0 = permittivity of vacuum, $C^2/N^{-1}/m^{-2}$

e = electron charge, C

and

$$G(\xi) = \frac{\phi(\xi) - \xi \dfrac{d\phi}{d\xi}}{2\xi^2} \tag{2}$$

with

$$\xi = \left(\frac{\epsilon_p}{kT_e}\right)^{1/2}$$

and

$$\phi(\xi) = \frac{2}{\pi^{1/2}} \int_0^{\xi} e^{-y^2}\, dy \tag{3}$$

$G(\xi)$ has been tabulated by Spitzer (Ref. 8). Equation (1) is plotted in Fig. 2 for a range of electron energies for $n_e = 10^{11}$ cm^{-3}. This time can easily be estimated for other densities, since $\ln \Lambda$ varies slowly with n_e.

The time between primary electron–ion collisions can be determined from the equation (Ref. 8)

$$\tau_{ei} = \frac{3.2 \times 10^4\, \epsilon_p^{3/2}}{n_e\, [\phi(\xi) - G(\xi)] \ln \Lambda} \tag{4}$$

where the terms are defined as before. The $\ln \Lambda$ factor is again found from the Maxwellian electron group, since it involves the Debye length determined by the Maxwellian electron temperature. This time is plotted in Fig. 3 for $n_e = 10^{11}$ cm^{-3}.

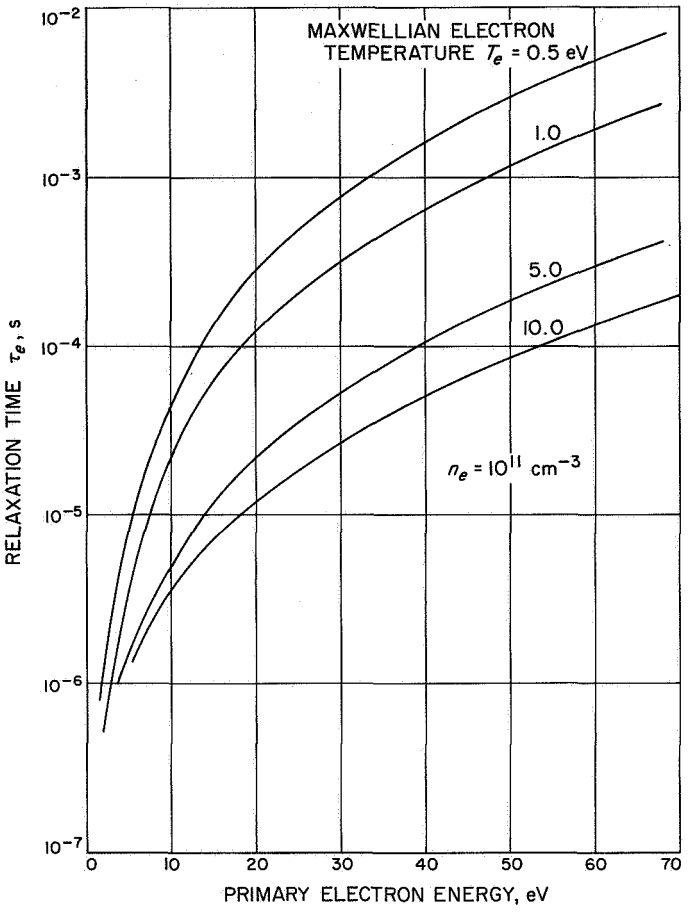

Fig. 2. Primary electron relaxation time

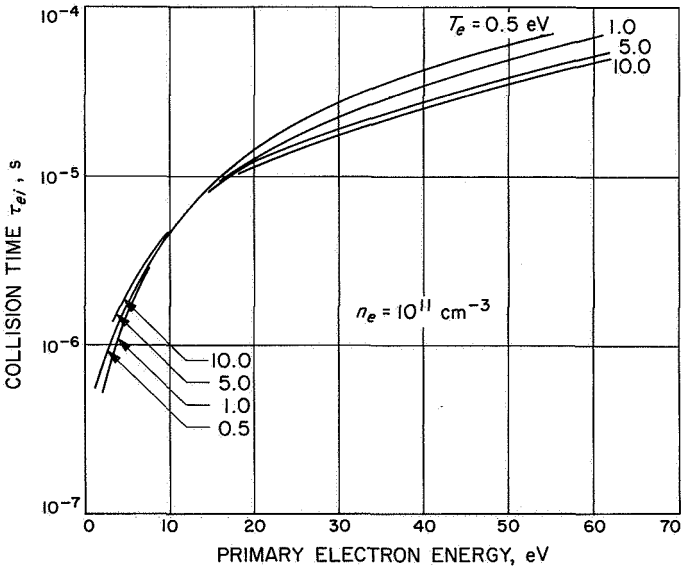

Fig. 3. Primary electron–ion collision times

The time between electron–electron collisions within the Maxwellian group can be computed from the "self-collision" time equation (Ref. 8)

$$\tau_m = 1.8 \times 10^5 \frac{\epsilon_m^{3/2}}{n_e \ln \Lambda} \tag{5}$$

where ϵ_m is the average Maxwellian electron energy in electron volts. This collision time is plotted in Fig. 4 for a range of electron densities and average energies. Maxwellian electron–ion elastic collision times are essentially those for electron–electron collisions (Ref. 9). The electron–ion energy exchange times, however, should be long compared to electron–electron energy exchange times, since energy is transferred more effectively between electrons. Electron–ion relaxation is therefore neglected. The electrons are assumed to have much higher temperatures than the ions; thus, the plasma is not in thermal equilibrium.

A note is needed here to point out the convention used in describing electron temperature. When temperature

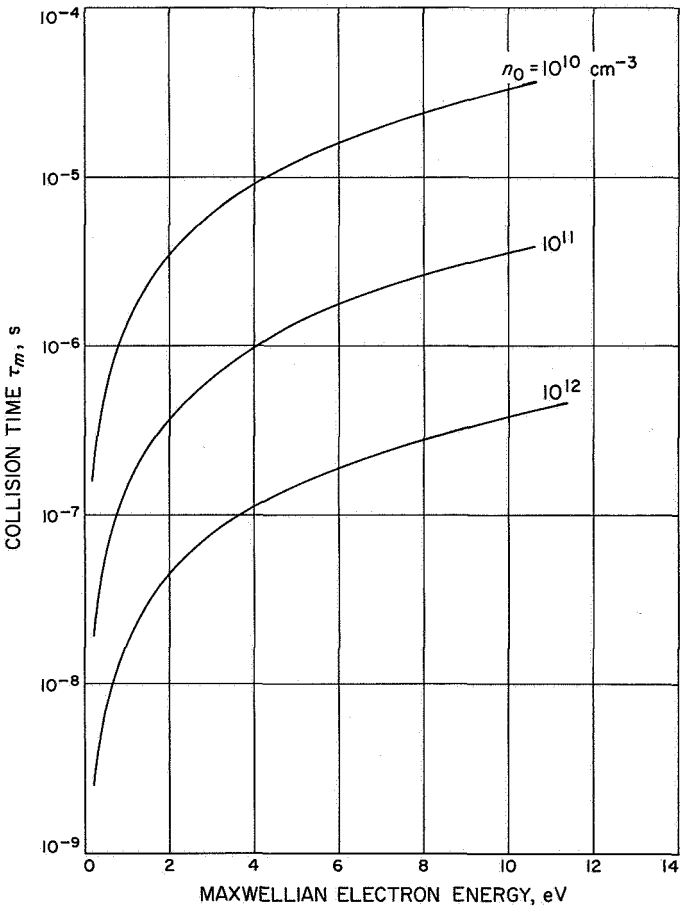

Fig. 4. Maxwellian electron self collision times

is discussed, it is understood that either degrees Kelvin are to be used, or the electron volt equivalent $e/k = 11{,}600°K/V^{-1}$ in conversion when T_e is given in electron volts. When electron energy is discussed in electron volts, the conversion $(3/2)kT_e$ must be used to find T_e. This distinction is made because the Langmuir probe measurements described later give T_e in electron volts and should not be confused with the average energy of the Maxwellian distribution.

The inelastic electron–atom collision times can be computed from (Ref. 9)

$$\tau_{ea} = \frac{1}{n_0 Q_{ea} V_e} \tag{6}$$

where

n_0 = neutral atom density, cm^{-3}

Q_{ea} = inelastic collision cross section, cm^2

V_e = electron speed, cm/s^{-1}

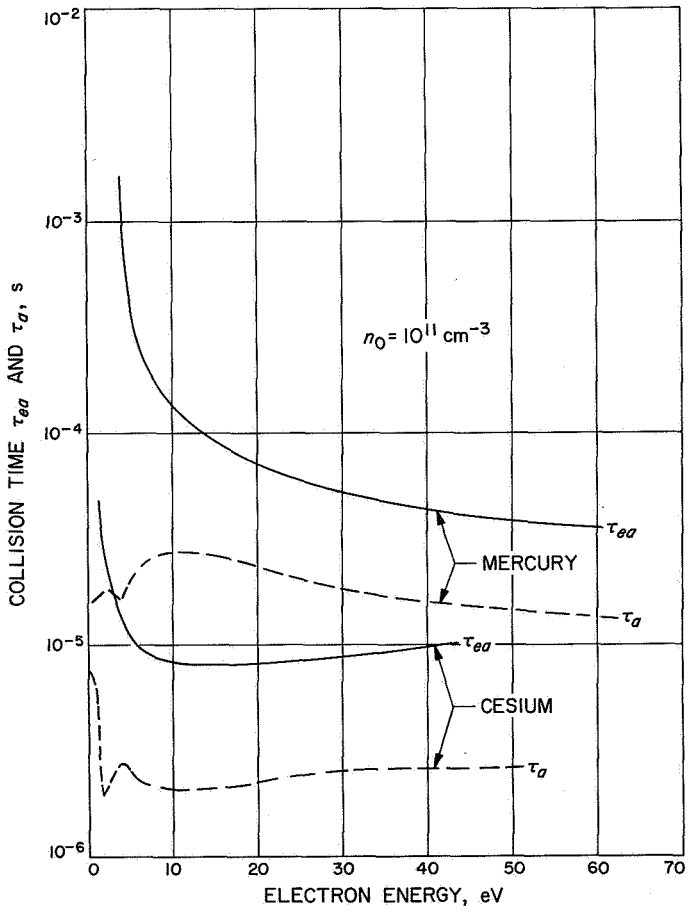

Fig. 5. Elastic and inelastic electron–atom collision times

The cross section Q_{ea} includes ionization and excitation. Sovie and Dugan (Ref. 10) have calculated τ_{ea} for cesium using Gryzinski's classical theory (Ref. 11); their curve is shown in Fig. 5. The mercury calculation, also plotted in Fig. 5, was made using the experimental data of Refs. 12 and 13 to form the inelastic cross section (Fig. 6). The cesium curve was obtained by using Eq. (6) and the collision times of Ref. 10.

The time between elastic electron–atom collisions is pertinent in determining the time required for electrons to be scattered without energy exchange. Since the electron–ion collisions are also essentially elastic, the faster of the electron–atom or electron–ion collision times should determine scattering. The electron–atom collision time τ_a can be estimated by using an equation similar to Eq. (6) with the total collision cross section. The total cross sections (Refs. 14 and 15) are shown in Figs. 7 and 8, and the times are shown in Fig. 5 for $n_0 = 10^{11}$ cm^{-3}. The upper right curve in Fig. 8 was used in calculating the cesium collision times. The various curves and data points in this figure are referenced in Ref. 15 and serve to show the wide variation in reported cross sections.

The arc voltages in the cesium and mercury engine are typically 10 and 50 V, respectively (Refs. 16 and 17). The primary electrons are found to have energies about equal to the arc voltage, and the Maxwellian electrons about

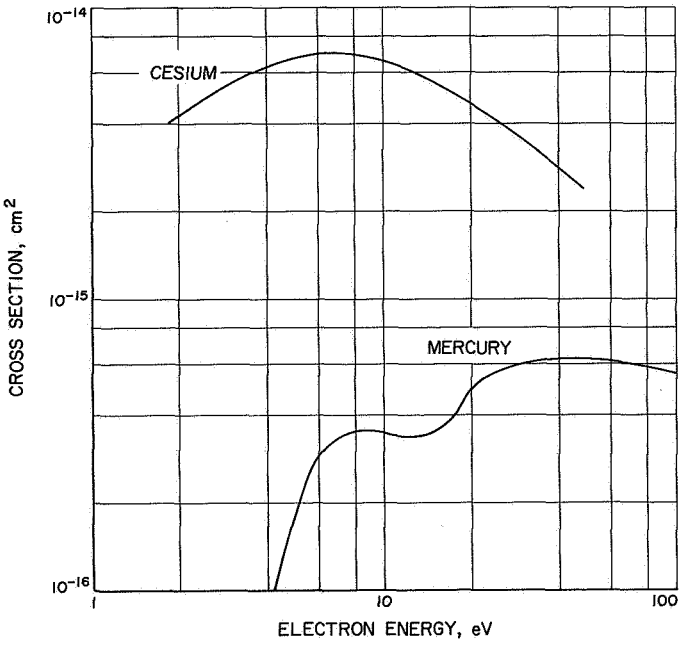

Fig. 6. Inelastic electron–atom collision cross sections for mercury (Refs. 12 and 13) and cesium (Ref. 10)

one-tenth the arc voltage (Ref. 18). Near the cathode, the plasma should be highly ionized. Assuming 90% ionization and an electron density of 10^{12} cm^{-3}, the various collision times (in seconds) for cesium and mercury are

Cs	Hg
$\tau_e = 2 \times 10^{-6}$	$\tau_e = 2 \times 10^{-5}$
$\tau_{ei} = 4 \times 10^{-7}$	$\tau_{ei} = 4 \times 10^{-6}$
$\tau_{ea} = 8 \times 10^{-6}$	$\tau_{ea} = 4 \times 10^{-5}$
$\tau_a = 2 \times 10^{-6}$	$\tau_a = 2 \times 10^{-5}$

(7)

An important characteristic of these plasmas is the relative concentration of primary and Maxwellian electrons. The population of primary electrons can be expressed as

$$n_p(r) = n_p(0)\, e^{-t/\tau} \tag{8}$$

where τ is the time required for energy exchange and $n_p(0)$ is the initial density. In order to compare the primary ratio $n_p(r)/n_p(0)$ for mercury and cesium, a discussion of t and τ of Eq. (8) is needed. For our purposes,

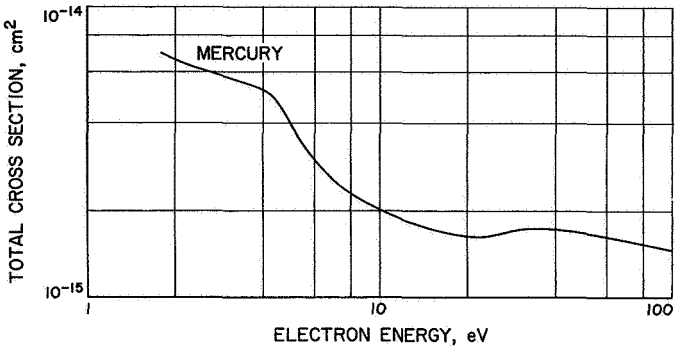

Fig. 7. Total electron–atom collision cross section for mercury (Ref. 14)

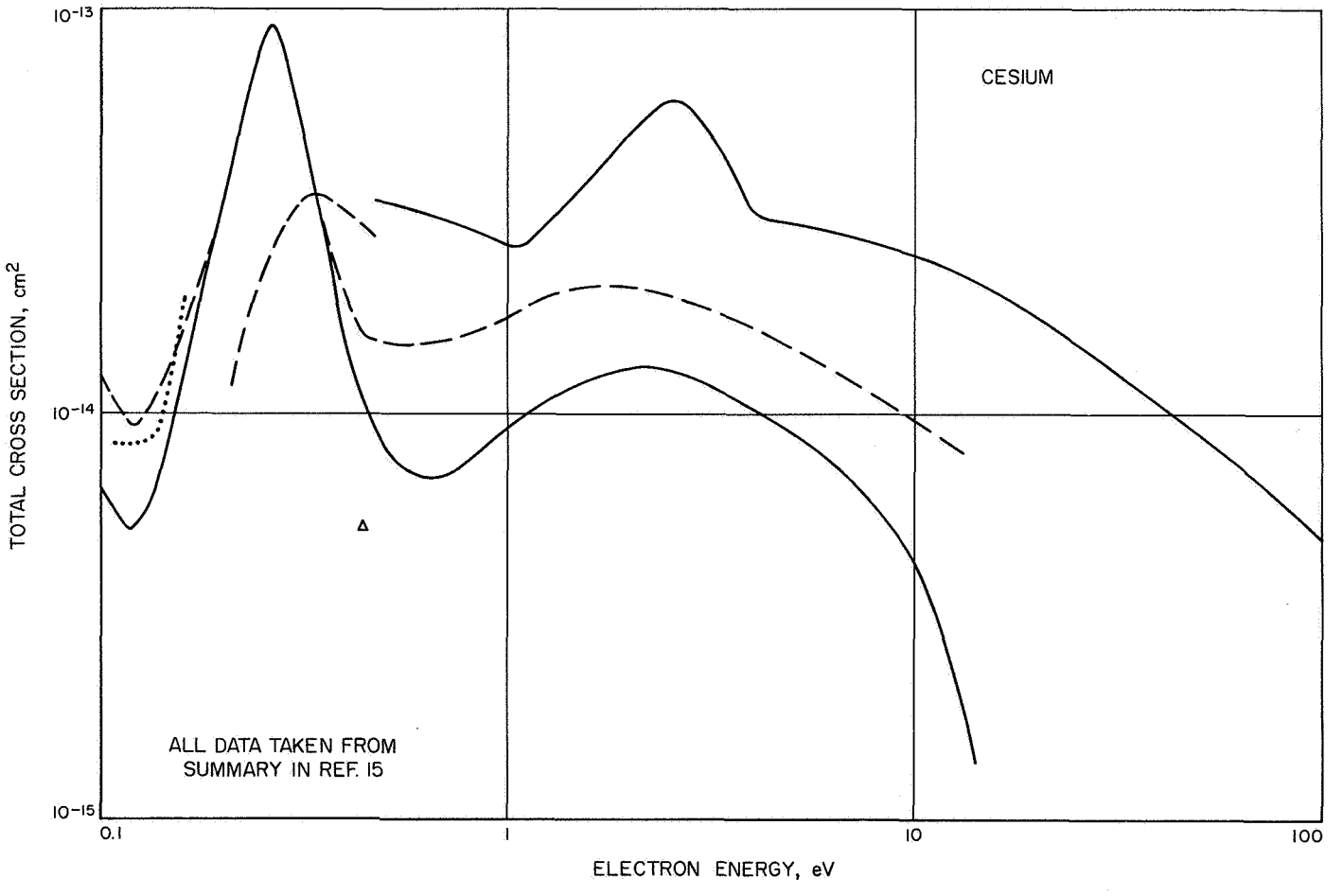

Fig. 8. Total electron–atom collision cross section for cesium (Ref. 15)

t will be taken as the time required for electrons to traverse the radius of the chamber and τ as the time required for primaries to join the Maxwellian distribution, or $\tau = \tau_e$. The traverse time will depend on a combination of the electron–atom or electron–ion times. Since the atom and ion densities vary radially, the relative importance of τ_{ei} and τ_a cannot be distinguished. Also, since the cross sections are relatively inaccurate for electron–atom collisions as indicated in Fig. 8, it is assumed that t is the same in both plasmas. The solid line in Fig. 9 shows a plot of Eq. (8) including only τ_e, and an estimate for electron energy loss because of collisions with atoms and ions shown by the dashed curve. The time t is interpreted as a distance divided by a velocity. The velocity is that determined by an electron moving one cyclotron radius per collision. Experimentally, the primary ratio at the anode, designated as point R, is approximately 10^{-3}. The dashed mercury curve is fairly representative of the measured primary distributions. The dashed cesium curve was estimated from the mercury curve. Considering the dashed curve for cesium, it is apparent that an extremely low fraction of primaries would be expected in cesium relative to mercury. It will be shown that in fact no primaries are detected in cesium plasma measurements.

The effectiveness of primary and Maxwellian electrons in producing ionization can be calculated following the method of Refs. 6 and 19. The production rate per unit volume is

$$\nu(r, \epsilon) = \frac{dn_i(r, \epsilon)}{dr} \tag{9}$$

where ν is the production rate at position r by electrons of energy ϵ. Assuming that the electron energy distribution function can be represented by

$$f(r, \epsilon) = f_p(\epsilon)\, n_p(r) + f_m(\epsilon)\, n_m(r) \tag{10}$$

where

$f_p(\epsilon)$ = primary electron distribution function

$= \delta(\epsilon_p)$ = delta function

$f_m(\epsilon)$ = Maxwellian distribution function

$n_p(r)$ = primary electron density at position r

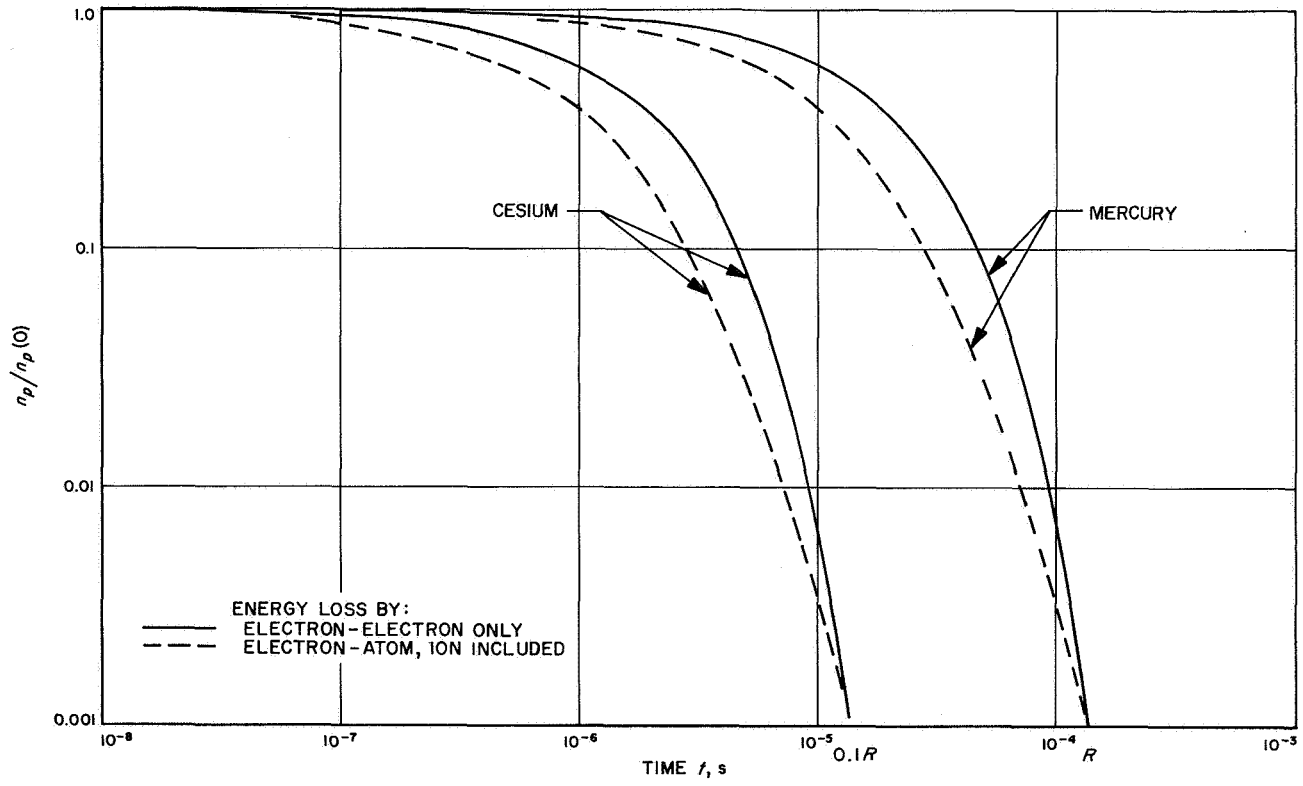

Fig. 9. Relative primary electron decay rate for mercury and cesium plasmas

the production rate is

$$\nu(r,\epsilon) = \left(\frac{2\epsilon}{m_e}\right)^{1/2} n_0(r)\, Q_i(\epsilon)\, f(r,\epsilon) \tag{11}$$

where Q_i is the ionization cross section for single ionization and $n_0(r)$ is the neutral particle density at position r.

Experimental measurements of Q_i for mercury and cesium are shown in Figs. 10 and 11 along with Gryzinski's theory (Refs. 13, 20, and 21). The theoretical curves were computed using

$$Q_i = \Sigma N_k Q_k \tag{12}$$

with

$$Q_k = \frac{6.56 \times 10^{-14}}{U_i^2}\, g(\zeta) \tag{13}$$

where U_i is the energy required to remove a single electron from the kth atomic state, N_k is the number of electrons in the kth state, $\zeta = \epsilon/U_i$,

$$g(\zeta) = \frac{1}{\zeta}\left(\frac{\zeta-1}{\zeta+1}\right)\left[1 + \frac{2}{3}\left(1 - \frac{1}{2\zeta}\right)\ln\left(2.7 + \sqrt{\zeta - 1}\right)\right] \tag{14}$$

and ϵ is the energy of the colliding electron. The ionization energies for each state are needed for this calculation and were obtained from Ref. 22 on atomic spectra. The notation on the theoretical curves designates the state, the number of electrons in the ground state configuration, and the energy required to remove an electron from that state. In the case of mercury, it is interesting to note the large contribution from the 5d state. The cesium experimental data were adjusted to match the theory as suggested by McFarland (Ref. 23).

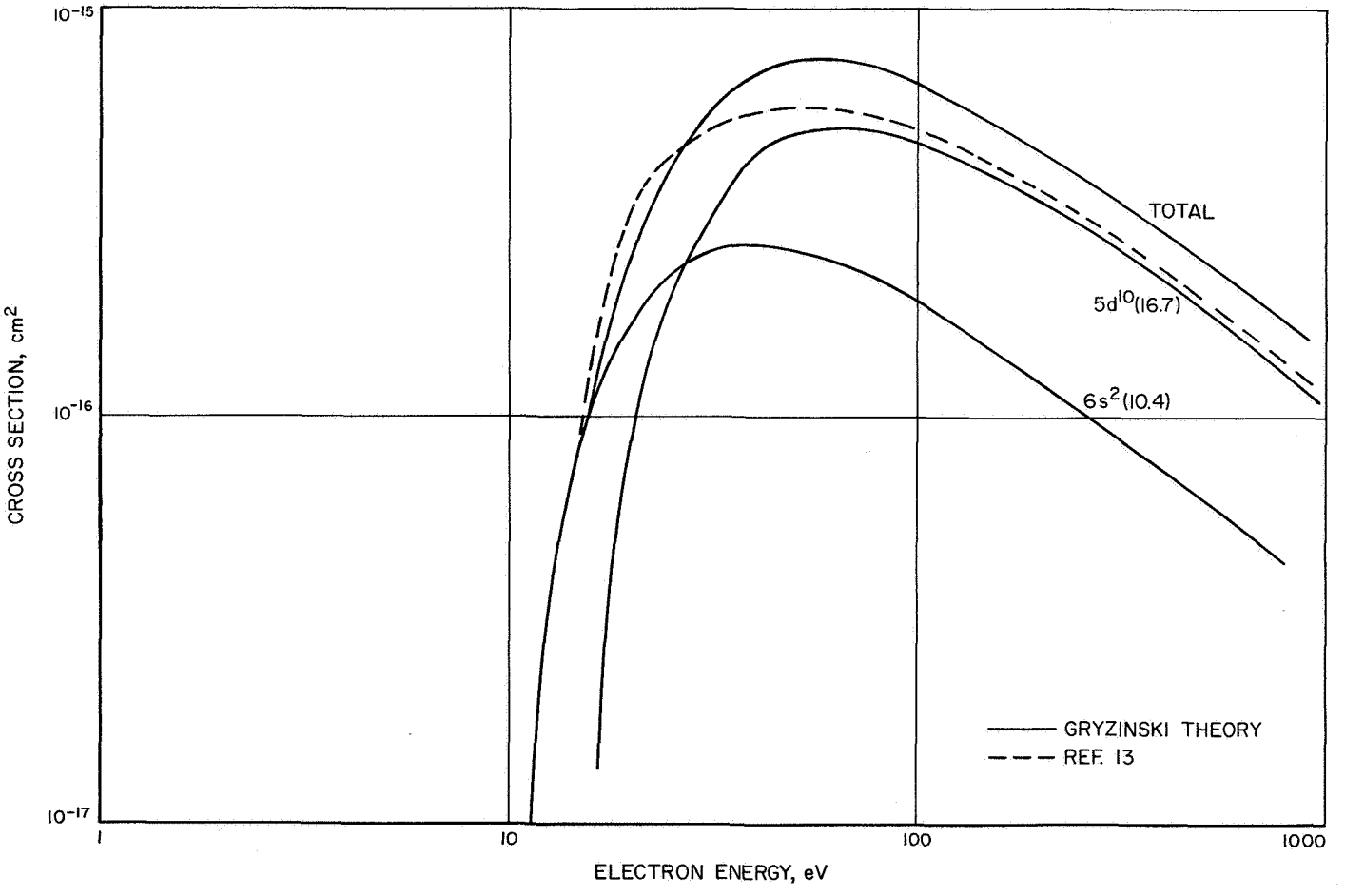

Fig. 10. Ionization cross section for producing singly charged mercury ions

Integration of Eq. (11) has been previously accomplished for mercury (Refs. 6, 19) using Eq. (10), and for cesium (Ref. 4) for a Maxwellian distribution alone. The integration yields

$$\nu(r) = \left(\frac{2}{m_e}\right)^{1/2} Q_i(\epsilon_p)\, n_0(r)\, n_p(r)\, \epsilon_p^{1/2} + \left(\frac{2}{m_e}\right)^{1/2} n_0(r)\, n_m(r)\, R_m \qquad (15)$$

where

$n_m(r)$ = Maxwellian electron density

and

$$R_m = \int_0^\infty f_m\, Q_i(\epsilon)\, \epsilon^{1/2}\, d\epsilon$$

Slightly different functions were used in Ref. 19. Equation (15) can be written as

$$\nu(r) = n_0(r)\,[n_p(r)\,\Sigma_p + n_m(r)\,\Sigma_m] \qquad (16)$$

where

$$\Sigma_p = \left(\frac{2}{m_e}\right)^{1/2} Q_i(\epsilon_p)\,\epsilon_p^{1/2} \qquad (17)$$

$$\Sigma_m = \left(\frac{2}{m_e}\right)^{1/2} R_m \qquad (18)$$

The functions Σ_p and Σ_m are shown in Fig. 12 for mercury and in Fig. 13 for cesium. The ionization cross section used in calculating Σ_m^{Cs} in Ref. 4 was not stated but should be accurate enough for our purpose here. Using the Maxwell and primary energies assumed before, the ion production coefficients Σ_p and Σ_m are about the same for

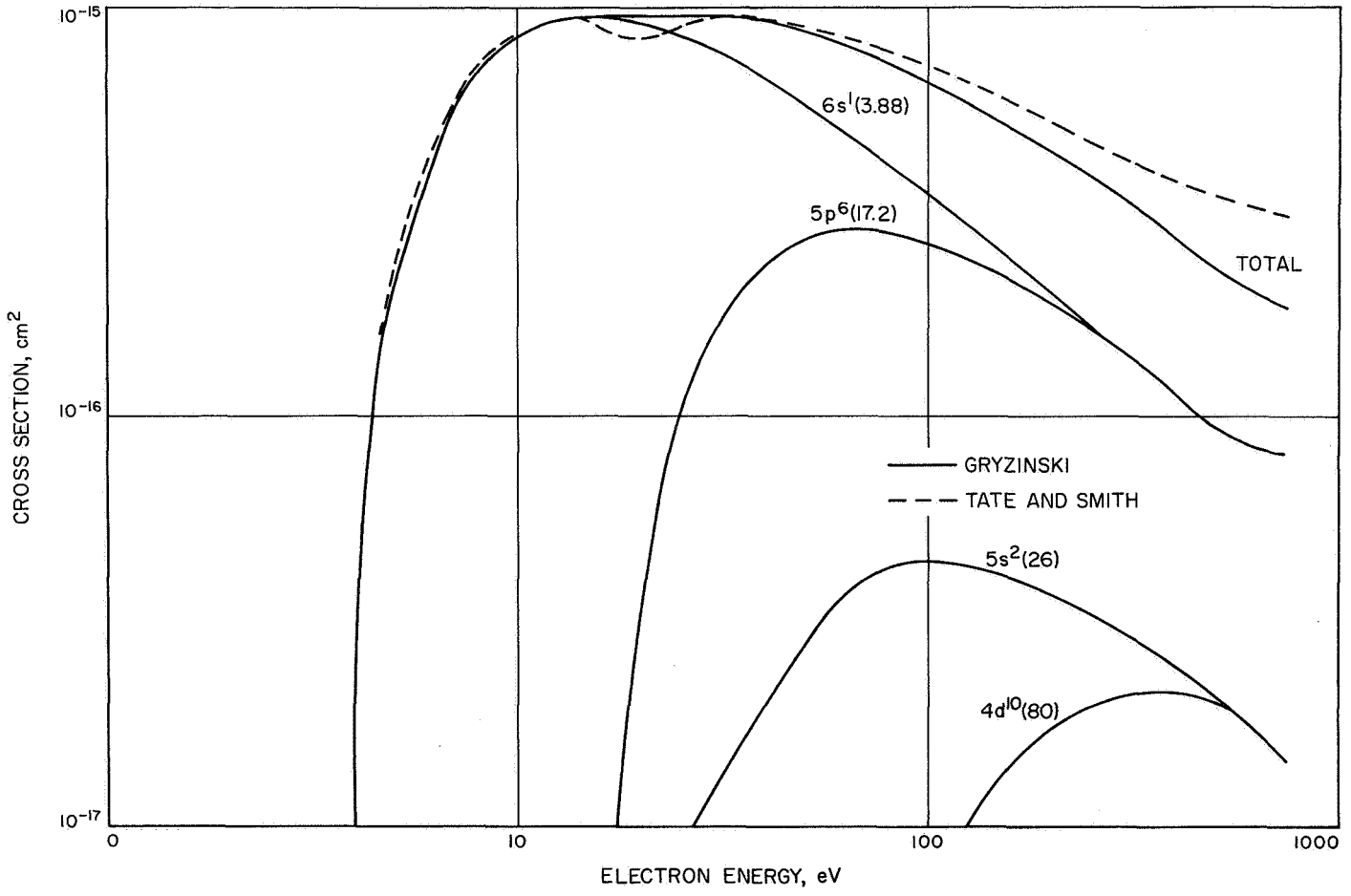

Fig. 11. Ionization cross section for producing singly charged cesium ions

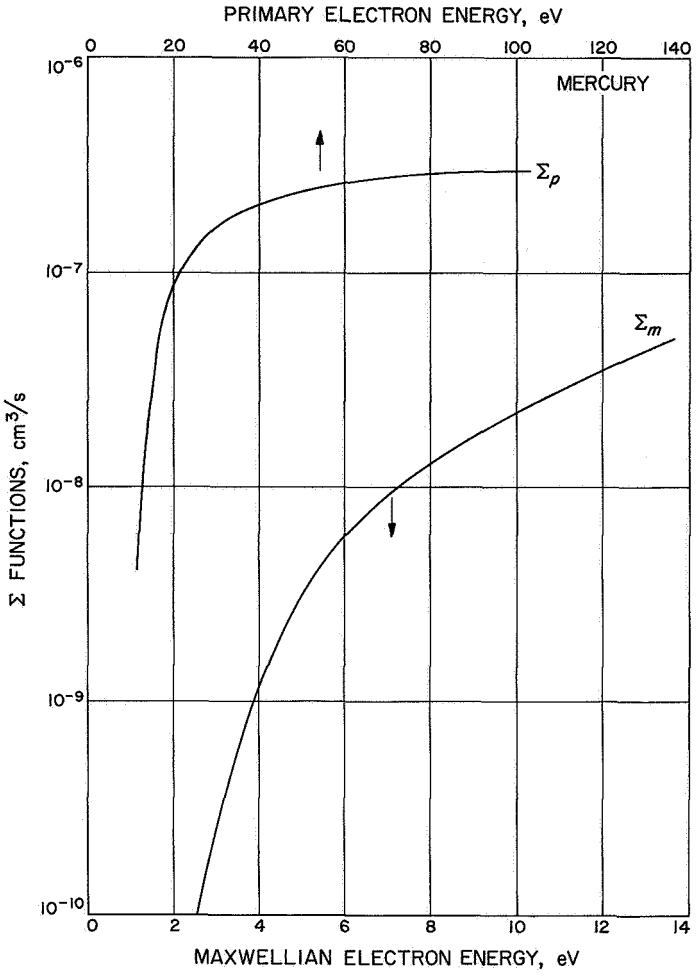

Fig. 12. Ion production coefficients for primary and Maxwellian electrons in mercury

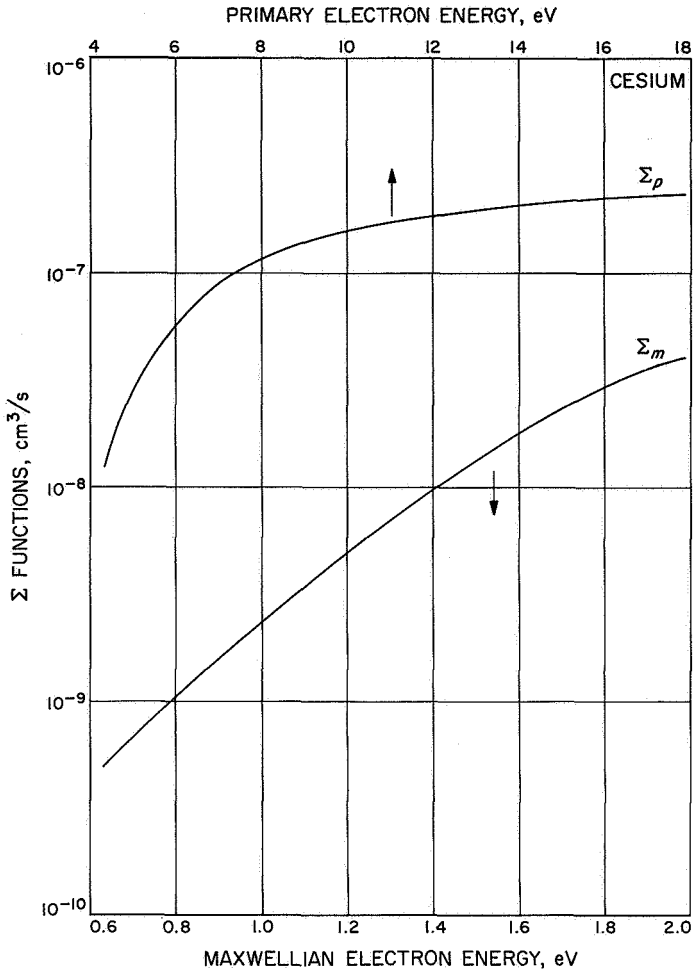

Fig. 13. Ion production coefficients for primary and Maxwellian electrons in cesium

mercury and cesium. However, there is quite a large difference in the effectiveness of Maxwellian and primary electrons. The production coefficients will be required for solving the ion and electron flux equations.

B. Diffusion Theory

The study of charged particle diffusion processes has been the subject of a great many investigations. Two comprehensive summary papers are available (Refs. 24 and 25) which list numerous references, so a general treatment of diffusion is not attempted in this paper. This section presents the equations required to describe the plasma in the electron bombardment engine, indicates the necessary assumptions, and outlines the solution. The equations presented have previously been solved with various simplifying assumptions (Refs. 24 and 25), but in most cases, these solutions do not aply to the problem of interest here. The following formulation assumes that the neutral particles are stationary and are included only as target particles for the charged species. The equations of motion for the charged particles can be written as (Ref. 24)

$$m_\alpha\left[\frac{\partial \mathbf{u}_\alpha}{\partial t} + \mathbf{u}_\alpha \cdot \nabla \mathbf{u}_\alpha\right] = Z_\alpha e\,(\mathbf{E} + \mathbf{u}_\alpha \times \mathbf{B}) - \frac{\nabla P_\alpha}{n_\alpha} + m_\alpha \frac{\delta \mathbf{u}_\alpha}{\delta t} \qquad (19)$$

where α denotes the species and

m_α = mass

$\mathbf{u}_\alpha$ = directed velocity

$Z_\alpha e$ = charge

$\mathbf{E}$ = electric field

$\mathbf{B}$ = magnetic field

P_α = hydrostatic pressure

n_α = number density

$\delta \mathbf{u}_\alpha / \delta t$ = momentum exchange term

The pressure can be written as

$$P_\alpha = \frac{2}{3} n_\alpha \epsilon_\alpha \tag{20}$$

which, for a Maxwellian energy distribution, is

$$P_\alpha = n_\alpha T_\alpha \tag{21}$$

where T_α = temperature in energy units. The momentum exchange term $\delta \mathbf{u}_\alpha / \delta t$ accounts for momentum transfer between species and can be written

$$m_\alpha \frac{\delta \mathbf{u}_\alpha}{\delta t} = -m_\alpha \sum_\beta \nu_{\alpha\beta} (\mathbf{u}_\alpha - \mathbf{u}_\beta) \tag{22}$$

where $\nu_{\alpha\beta}$ = collision frequency. An additional relationship accounting for the conservation of momentum in collisions is given by

$$n_\alpha m_\alpha \nu_{\alpha\beta} = n_\beta m_\beta \nu_{\beta\alpha} \tag{23}$$

In addition to the equations of motion, the species continuity equation must be satisfied

$$\nabla \cdot \mathbf{\Gamma}_\alpha = \nu_i^\alpha - \nu_r^\alpha \tag{24}$$

in which

$\mathbf{\Gamma}_\alpha = n_\alpha \mathbf{u}_\alpha$

ν_i^α = species production rate

ν_r^α = species recombination rate

The production function ν_i^α is that previously calculated, and the Σ functions could be conveniently used in the numerical solutions. Recombination in the plasma, represented by ν_r^α, should be small compared to production (Refs. 19 and 26) and can be neglected. The recombination at surfaces, however, will have to be included in boundary conditions. Finally, it is necessary to examine the Maxwell equations. These can be written as

$$\nabla \cdot \mathbf{E} = [n_i - (n_m + n_p)] \frac{e}{\epsilon_0} \tag{25}$$

$$\nabla \times \mathbf{E} = 0 \tag{26}$$

$$\nabla \cdot \mathbf{B} = 0 \tag{27}$$

$$\nabla \times \mathbf{B} = e\mu_0 [\mathbf{\Gamma}_i - (\mathbf{\Gamma}_m + \mathbf{\Gamma}_p)] \tag{28}$$

where $\mu_0 = 12.57 \times 10^{-7}$ W/A^{-1}/m^{-1}.

The momentum transfer equations can be simplified by eliminating the terms on the left-hand side of Eq. (19), and this is the usual procedure. The elimination of $\partial \mathbf{u}_\alpha / \partial t$ is certainly justified, since the plasma is known to be in a steady-state condition. In the case of the electrons, the term in $(\mathbf{u} \cdot \nabla)\mathbf{u}$ can also be eliminated, based on the experimental fact that thermal electron velocities far exceed the directed velocity. The directed velocity is in turn determined by the elastic electron–atom and electron–ion collision rates. These rates can be assumed to remain relatively constant across the plasma, leading to a constant drift velocity; hence, $(\mathbf{u}_e \cdot \nabla)\mathbf{u}_e = 0$ is a reasonable assumption.

In the case of the ions, however, a different situation exists. Ionic cyclotron radii are very large compared with the dimensions of the device, so the magnetic field has no effect on them. Further, for the plasmas under consideration, the mean free path of ions for momentum transfer is also large in comparison to the dimensions of the device, and the ionic thermal velocity is quite low. Thus, the existence of any appreciable potential gradients in the plasma would result in ion acceleration, and an equilibrium drift velocity could not be reached. Experimentally, such gradients are known to exist, so the term $(\mathbf{u}_i \cdot \nabla)\mathbf{u}_i$ should be retained in the ion equation of motion. This term is nonlinear and makes an analytic solution impossible. The term $\delta \mathbf{u}_\alpha / \delta t$ will produce a term μ_i, defined as the mobility due to ion–atom collisions. In the case of long ion mean free paths, the entire concept of mobility is questionable.Because the ionic drift velocity is expected to be small compared to electron velocities, it is not unreasonable to lump the effects of $(\mathbf{u}_i \cdot \nabla)\mathbf{u}_i$ into the ion mobility and treat this mobility as a parameter. The solutions can then be adjusted by means of μ_i to fit experimental data. Such solutions would be valid only if the mobility so determined were consistent in both the radial and axial solutions.

The primary electron, Maxwellian electron, and ion-equations of motion will now be presented. They will then be simplified with the use of the following additional assumptions: (1) The primary electrons only affect the plasma near the cathode and can be neglected in the bulk of the plasma. The neglect of primary electrons in cesium is experimentally justified; but this assumption must be

verified for mercury. (2) The ion and electron densities are equal locally, and Eq. (25) is neglected (Ref. 27). (3) The magnetic field is constant and has only an axial (z) component. (4) There is no azimuthal electric field or density gradient, although these terms are included for generality. (5) The temperatures are constant but not equal. Both the electron and ion temperatures are carried as far as possible within the differential. (6) Plasma currents are small enough not to affect the applied magnetic field; thus, Eqs. (27) and (28) can be eliminated. (7) The ion density is a separable function of coordinates, so that Eq. (26) can be neglected as indicated in Ref. 27.

The individual species equations of motion for ions, Maxwellian electrons, and primary electrons can be written in the following manner:

Ions

$$e\mathbf{E} + e\mathbf{u}_i \times \mathbf{B} = \frac{\nabla P_i}{n_i} + m_i \nu_{im}(\mathbf{u}_i - \mathbf{u}_m) + m_i \nu_{i0}\mathbf{u}_i + m_i \nu_{ip}(\mathbf{u}_i - \mathbf{u}_p) \tag{29}$$

Maxwellian electrons

$$-e\mathbf{E} - e\mathbf{u}_m \times \mathbf{B} = \frac{\nabla P_m}{n_m} + m_e \nu_{mi}(\mathbf{u}_m - \mathbf{u}_i) + m_e \nu_{mp}(\mathbf{u}_m - \mathbf{u}_p) + m_e \nu_{m0}\mathbf{u}_m \tag{30}$$

Primary electrons

$$-e\mathbf{E} - e\mathbf{u}_p \times \mathbf{B} = \frac{\nabla P_p}{n_p} + m_e \nu_{pi}(\mathbf{u}_p - \mathbf{u}_i) + m_e \nu_{pm}(\mathbf{u}_p - \mathbf{u}_m) + m_e \nu_{p0}\mathbf{u}_p \tag{31}$$

We now make use of the definitions

$$\eta_m = \frac{m_e \nu_{mi}}{n_m e^2} \qquad \eta_{pm} = \frac{m_e \nu_{pm}}{n_p e^2}$$

$$\eta_p = \frac{m_e \nu_{pi}}{n_p e^2} \qquad \mu_m = \frac{e}{m_e \nu_{m0}}$$

$$\mu_i = \frac{e}{m_i \nu_{i0}} \qquad \mu_p = \frac{e}{m_e \nu_{p0}} \tag{32}$$

where η = resistivity and μ = mobility, and of Eq. (23) to find

$$n_i \mathbf{E} + \boldsymbol{\Gamma}_i \times \mathbf{B} = \nabla(n_i T_i) + \eta_m n_m e\left(\frac{n_m}{n_i}\boldsymbol{\Gamma}_i - \boldsymbol{\Gamma}_m\right) + \eta_p n_p e\left(\frac{n_p}{n_i}\boldsymbol{\Gamma}_i - \boldsymbol{\Gamma}_p\right) + \frac{\boldsymbol{\Gamma}_i}{\mu_i} \tag{33}$$

$$-n_m \mathbf{E} - \boldsymbol{\Gamma}_m \times \mathbf{B} = \nabla(n_m T_m) + \eta_m n_m e\left(\boldsymbol{\Gamma}_m - \boldsymbol{\Gamma}_i \frac{n_m}{n_i}\right) + \eta_{pm} n_p e\left(\frac{n_p}{n_m}\boldsymbol{\Gamma}_m - \boldsymbol{\Gamma}_p\right) + \frac{\boldsymbol{\Gamma}_m}{\mu_m} \tag{34}$$

$$-n_p \mathbf{E} - \boldsymbol{\Gamma}_p \times \mathbf{B} = \frac{2}{3}\nabla(n_p \epsilon_p) + \eta_p n_p e\left(\boldsymbol{\Gamma}_p - \frac{n_p}{n_i}\boldsymbol{\Gamma}_i\right) + \eta_{pm} n_p e\left(\boldsymbol{\Gamma}_p - \frac{n_p}{n_m}\boldsymbol{\Gamma}_m\right) + \frac{\boldsymbol{\Gamma}_p}{\mu_p} \tag{35}$$

Note that μ_i is now the "effective" mobility and cannot be computed using the ion–atom collision times of Section A. The primary electrons are neglected as indicated previously, and the ion and Maxwellian electron equations are reduced with the definitions $\eta_m = \eta$ and $n_i = n_m = n$.

$$-\boldsymbol{\Gamma}_i \times \mathbf{B} - n\mathbf{E} + \nabla(n_i T_i) = -\frac{\boldsymbol{\Gamma}_i}{\mu_i} + \eta e n(\boldsymbol{\Gamma}_e - \boldsymbol{\Gamma}_i) \tag{36}$$

$$\boldsymbol{\Gamma}_e \times \mathbf{B} + n\mathbf{E} + \nabla(nT_e) = -\frac{\boldsymbol{\Gamma}_e}{\mu_e} - \eta e n(\boldsymbol{\Gamma}_e - \boldsymbol{\Gamma}_i) \tag{37}$$

The components of Eqs. (36) and (37) for the r-, θ-, and z-directions are:

r-direction

$$-\Gamma_\theta^i B - nE_r + \frac{\partial}{\partial r}(nT_i) = -\frac{\Gamma_r^i}{\mu_i} + \eta e n(\Gamma_r^e - \Gamma_r^i) \tag{38}$$

$$\Gamma_\theta^e B + nE_r + \frac{\partial}{\partial r}(nT_e) = -\frac{\Gamma_r^e}{\mu_e} - \eta e n(\Gamma_r^e - \Gamma_r^i) \tag{39}$$

θ-direction

$$\Gamma_r^i B - nE_\theta + \frac{1}{r}\frac{\partial}{\partial\theta}(nT_i) = -\frac{\Gamma_\theta^i}{\mu_i} + \eta en(\Gamma_\theta^e - \Gamma_\theta^i) \quad (40)$$

$$-\Gamma_r^e B + nE_\theta + \frac{1}{r}\frac{\partial}{\partial\theta}(nT_e) = -\frac{\Gamma_\theta^e}{\mu_e} - \eta en(\Gamma_\theta^e - \Gamma_\theta^i) \quad (41)$$

z-direction

$$-nE_z + \frac{\partial}{\partial z}(nT_i) = -\frac{\Gamma_z^i}{\mu_i} + \eta en(\Gamma_z^e - \Gamma_z^i) \quad (42)$$

$$nE_z + \frac{\partial}{\partial z}(nT_e) = -\frac{\Gamma_z^i}{\mu_e} - \eta en(\Gamma_z^e - \Gamma_z^i) \quad (43)$$

These are the same equations as those derived in Ref. 27 using the Boltzmann transport equation. An interesting feature of the equations is that the z-direction equations are uncoupled from the r and θ equations.

The r and θ equations (38–41) can now be solved for the radial plasma potential distribution. This is accomplished by making the assumptions that the mobilities are constant and that $\Gamma_\theta^i << \Gamma_\theta^e$. Ecker (Ref. 28) has also solved these equations assuming that $\Gamma_r^e = \lambda\Gamma_r^i$, where λ is a constant, and the ratio of Γ_θ^i to Γ_θ^e is found to be

$$\frac{\Gamma_\theta^i}{\Gamma_\theta^e} = \left[\frac{1 + \sigma_e(1-\lambda)}{-\lambda + \sigma_i(1-\lambda)}\right]\frac{\mu_i}{\mu_e} \quad (44)$$

where

$$\sigma_{i,e} = \eta en\mu_{i,e} \quad (45)$$

It is seen that for λ equal to unity, the flux ratio is just equal to the mobility ratio. For λ different from unity, the flux ratio is between μ_i/μ_e and σ_i because $\sigma_i << 1 < \sigma_e$. Thus, for all conditions of interest here, the assumption of $\Gamma_\theta^i << \Gamma_\theta^e$ is well justified. The μ_i in the θ equation is actually a different mobility from those for the r- and z-directions because of the general tensor quality of the mobility. This is because ions have infinite path lengths available in the θ-direction, whereas their path is limited to the dimensions of the engine in r and z. In addition, the θ electric field is assumed to be zero, so μ_i^o is a zero field mobility (Refs. 29 and 30). For these reasons, the θ mobility should be large compared to those for the r- and z-directions. The Γ_θ^i term can therefore be eliminated in Eq. (38), because $\Gamma_\theta^i B << \Gamma_r^i/\mu_i^r$ and Γ_θ^i is neglected in Eq. (40) since $\Gamma_r^i B >> \Gamma_\theta^i/\mu_i^o$. The value of eliminating Γ_θ^i from the equations is that an additional relationship between fluxes is now unnecessary and the number of parameters in the radial solution is reduced to one (μ_i).

It will be assumed that μ_i is the same for r and z because of similar electric fields. It is further assumed that the Einstein relation holds, so that

$$D_{i,e} = \mu_{i,e} T_{i,e} \quad (46)$$

For constant temperatures, the θ equations (Eqs. 40 and 41) can now be solved for Γ_r^e as

$$\Gamma_r^e = \frac{1 + \sigma_e}{\sigma_e}\Gamma_r^i \quad (47)$$

Note that σ_e is a function of r, so that Γ_r^e is a changing function of Γ_r^i in addition to being non-ambipolar. Using Eqs. (38), (39), and (47) with the convention

$$E_r = -\frac{\partial V}{\partial r} \quad (48)$$

where V is the plasma potential, we find

$$-\frac{\partial V}{\partial r} = \left[\frac{D_i(1+u_e^2) + D_e(\sigma_i - \sigma_e) + 2\sigma_e D_i}{\mu_i(1+u_e^2) + \mu_e(\sigma_e - \sigma_i) + 2\sigma_e\mu_i}\right]\frac{1}{n}\frac{\partial n}{\partial r} \quad (49)$$

where

$$u = \mu B$$

We define a new variable

$$x = \frac{n(0)}{n} = \frac{\sigma(0)}{\sigma} \quad (50)$$

and integrate Eq. (49) to obtain

$$\frac{\Delta V^r}{T_e} = a_1 \ln x + a_2 \ln\left(\frac{1 + a_3 x}{1 + a_3}\right) \quad (51)$$

where

$$\Delta V = V(x) - V(1)$$

$$a_1 = \frac{1}{\bar{\mu}}\left(1 - \frac{\mu_e}{\mu_i} - 2\frac{T_i}{T_e}\right) \quad (52)$$

$$a_2 = \frac{1}{\bar{\mu}}\left[\frac{T_i}{T_e}(\bar{\mu} + 2) + \left(\frac{\mu_e}{\mu_i} - 1\right)\right] \quad (53)$$

$$a_3 = \frac{1 + u_e^2}{\sigma_{e0}\bar{\mu}} \quad (54)$$

$$\bar{\mu} = 1 + \frac{\mu_e}{\mu_i} \quad (55)$$

Under most conditions, $\mu_e/\mu_i >> 1$, so the constants become

$$a_1 = -1 \tag{56}$$

$$a_2 = 1 + \frac{T_i}{T_e} = \overline{T} \tag{57}$$

$$a_3 = \frac{\mu_i B^2}{\eta e n(0)} \tag{58}$$

The radial solution in Eq. (51), using the constants of Eqs. (56), (57), and (58), is compared to experimental data in Section III.

The axial potential distribution is easier to find. By using just the z-direction equations (Eqs. 42 and 43), and a relation between the fluxes

$$\Gamma_z^e = \gamma \Gamma_z^i \tag{59}$$

and Eqs. (45) and (46), the axial electric field is found to be

$$E_z = \left(\frac{D_i \alpha - D_e \beta}{\mu_i \alpha + \mu_e \beta}\right) \frac{1}{n} \frac{\partial n}{\partial r} \tag{60}$$

where

$$\alpha = [\gamma + \sigma_e(\gamma - 1)] \tag{61}$$

$$\beta = [1 - \sigma_i(\gamma - 1)] \tag{62}$$

Integration of Eq. (60) gives the axial potential in the form

$$\frac{\Delta V^z}{T_e} = b_1 \ln x + b_2\left(\frac{1}{x} - 1\right) \tag{63}$$

$$\Delta V^z = V(x) - V(1)$$

and

$$b_1 = \frac{\gamma(D_i/D_e) - 1}{1 + \gamma(\mu_i/\mu_e)} \tag{64}$$

$$b_2 = (1 - \gamma)\sigma_{i0}\overline{T}[1 + \gamma(\mu_i/\mu_e)] \tag{65}$$

As before, when $\mu_e/\mu_i >> 1$, the constants become

$$b_1 = -1 \tag{66}$$

$$b_2 = (1 - \gamma)\sigma_{i0}\overline{T}$$

This solution will also be discussed with the experimental data.

As indicated, the ion mobility will be determined by matching the radial solution, Eq. (51), to experimental data. This value of μ_i will then be used to fit the axial potential solution, Eq. (63). Both solutions require the resistivity due to electron–ion collisions, which is given by (Ref. 8)

$$\eta = \frac{6.53 \times 10^3}{T_e^{3/2}} \ln \Lambda \quad \Omega/\text{cm} \tag{67}$$

where T_e is in degrees Kelvin. The simplified plasma potential equations are presented for each engine comparison, since the a and b constants depend on the electron and ion temperatures in each experiment. The measured density distribution is relatively accurate, so that with the solution for the plasma potential, the characteristics of the plasma can be firmly predicted. The assumption of constant temperatures will be discussed with the experimental data. To include a variable electron or ion temperature, an energy equation for each species would be required.

C. Axial Ion Flux

The ion flux at the grid structure of the engine is important because it determines the ion beam current that can be extracted. The ion flux in the axial direction in the plasma is given by Eq. (42), using (59) as

$$\Gamma_z^i = \mu_i\left[nE_z - T_i\frac{\partial n}{\partial z}\right][1 + \sigma_i(1 - \gamma)]^{-1} \tag{68}$$

Using the definition of the potential, we find

$$\Gamma_z^i = -\mu_i\left[n\frac{\partial V}{\partial z} + T_i\frac{\partial n}{\partial z}\right][1 + \sigma_i(1 - \gamma)]^{-1} \tag{69}$$

With Eqs. (63) and (66), Γ_z^i becomes

$$\Gamma_z^i = -\mu_i T_e \overline{T}\frac{\partial n}{\partial z} \tag{70}$$

The form of Eq. (70) permits easy evaluation of Γ_z^i.

III. Plasma Measurements

The measurements made in three operating electron bombardment ion engines are now presented. Since a primary objective of this report is to evaluate the plasma theory, previously reported measurements are used as much as possible (Refs. 18, 31, and 32).

In the remaining discussion, the term "conventional" will refer to an engine geometry in which the cathode is in the center of the engine and the anode shape is annular. Two engines of this type will be discussed, a cylindrical and a conical one. The cylindrical engine has been operated on mercury and the conical engine on cesium. The third engine, also operated on cesium, will be referred to as the reversed-current engine because the cathode and anode geomety is inverted compared to the conventional geometry.

A. Experimental Method

All measurements were made with single movable Langmuir probes instrumented to plot the current–voltage traces automatically. Since the general Langmuir probe theory is well covered in the literature (Refs. 33 and 34), it will not be discussed in this report.

The equations used to reduce the experimental data are presented here for reference (Ref. 6). The Maxwellian electron density is calculated using

$$n_m = \frac{i_{sm}}{eA}\left(\frac{2\pi m_e}{kT_e}\right)^{1/2} \tag{71}$$

where

i_{sm} = Maxwellian electron current at the plasma potential

A = probe area

The primary electron density, when present in the plasma, is determined from

$$n_p = \frac{i_{sp}}{eA}\left(\frac{8m_e}{\epsilon_p}\right)^{1/2} \tag{72}$$

where i_{sp} = primary electron current at the plasma potential. The assumption of a monoenergetic group of primaries for the mercury plasma rather than a distribution of primary energy decreases the accuracy of the reduced data. The cesium data appear to be entirely Maxwellian, and thus no data-reduction problem occurs. The probe design is the same as that in Ref. 6, using a 0.020-in.-diameter tungsten wire with approximately 0.15 in. extending beyond the quartz sheath.

B. Cesium Measurements

The two engines operated on cesium are shown schematically in Figs. 14 and 15. The Langmuir probe positions are not indicated on the figures but will be evident from the data points presented later. The reversed geometry will be discussed first, since the measured electron temperatures were relatively constant and this engine most closely approximates the assumptions of the analysis.

1. Reversed-current engine. The data presented here are used only in conjunction with the model; a more complete description of the measurements is presented in Ref. 32. The electron temperature was found to be constant radially as indicated by Fig. 16. This figure shows that all probe traces fell on the same initial straight line and indicates a radially decreasing ion density and plasma potential. Axial measurements of electron temperature presented in Fig. 17 for three typical operating conditions also show a relatively constant electron temperature distribution. The radial ion density distribution data for five axial positions and one operating condition are given in Fig. 18. The conditions chosen for applying the potential solutions are

$$T_e = 0.7\,\text{eV} \qquad T_i/T_e = 0.1$$
$$n(0) = 10^{12}\,\text{cm}^{-3} \qquad n_0(0) = 10^{11}\,\text{cm}^{-3}$$
$$B = 5\,\text{G}$$

The radial potential solution (Eq. 51) reduces to

$$\Delta V = 0.7\left[1.1\ln\left(\frac{1+a_3 x}{1+a_3}\right) - \ln x\right] \tag{73}$$

and was found to fit the experimental data as shown in Fig. 19 for $\mu_i = 68\,\text{m}^2/\text{V}^{-1}/\text{s}^{-1}$ and a value of a_3 of 1.10. The axial solution reduces to

$$\Delta V = 0.7\left[1.5\times 10^{-2}(1-\gamma)\left(\frac{1}{x}-1\right) - \ln x\right] \tag{74}$$

The ion density of Fig. 18 is used to compute x, and the axial plasma potential is shown compared to the experimental data in Fig. 20. Note that the axial solution is essentially independent of γ because of the small coefficient (0.015). It is expected that γ would be between about 0.5 and 0.8 because the axial electron flux serves only to maintain neutrality for the ions lost in recombination at chamber surfaces. The relatively poor agreement of the axial solution with the measurements, in this case as well as those to be discussed, is attributed to variations in plasma conditions during the measurements. The experimental setup allowed complete sets of radial traces to be taken within a few minutes, while axial sets took nearly an hour. Thus, the radial data are consistent, but much scatter occurred in cross-plotting these data.

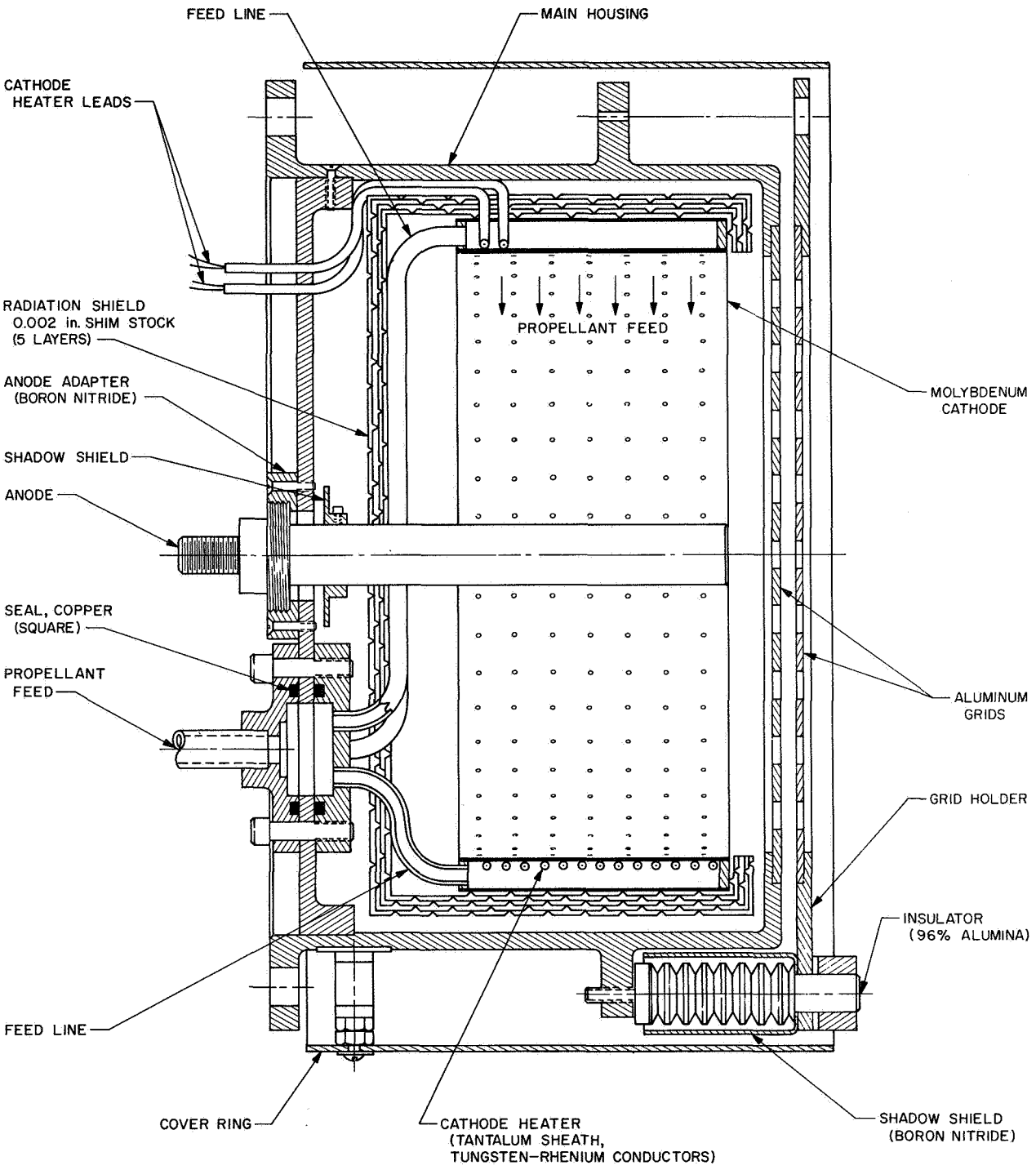

Fig. 14. Reversed arc current cesium electron bombardment ion engine

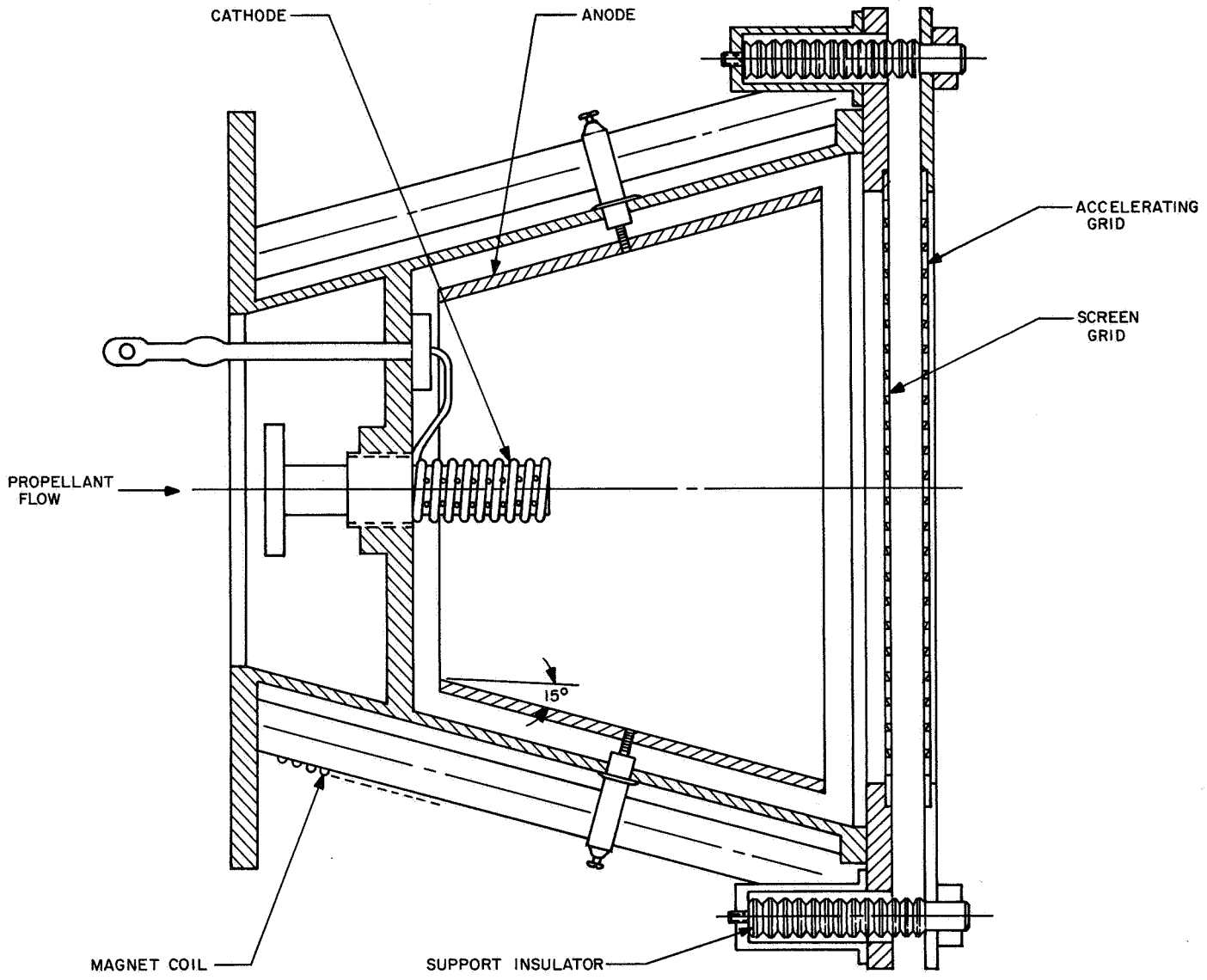

Fig. 15. Conical cesium electron bombardment ion engine

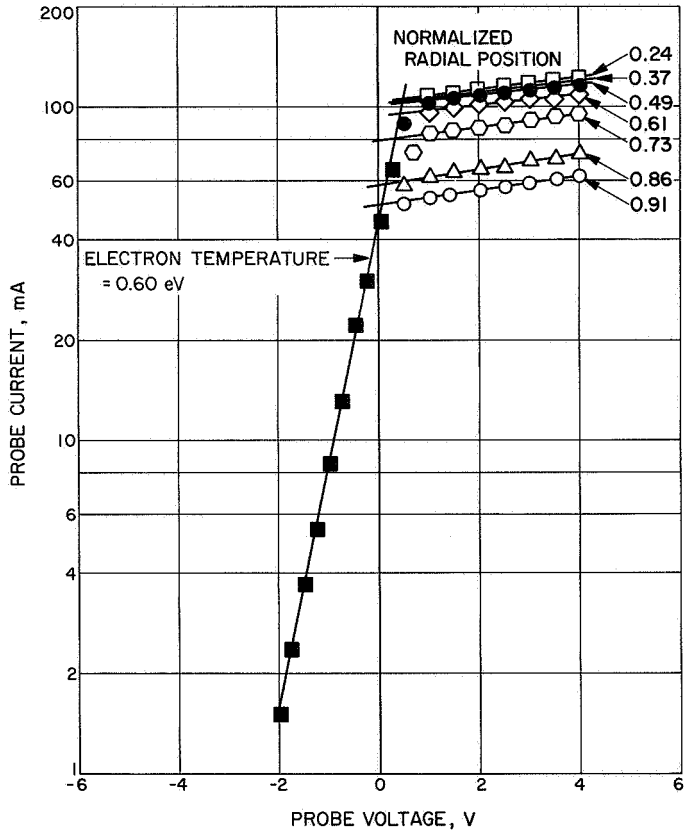

Fig. 16. Typical Langmuir probe semilogarithmic plot in cesium for seven radial positions

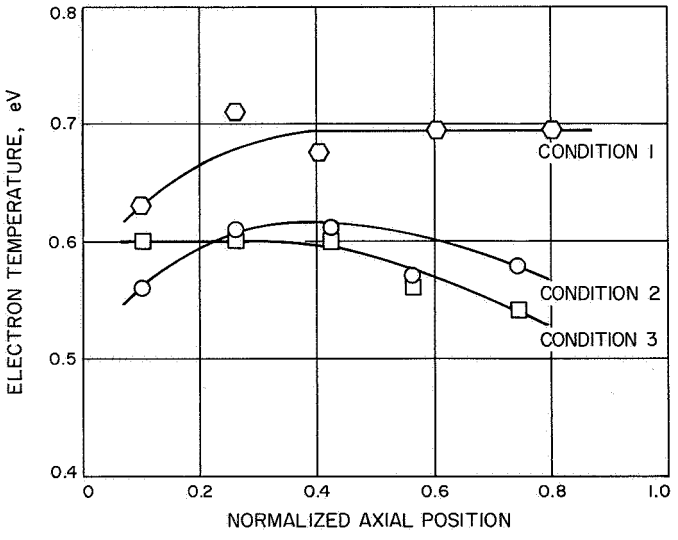

Fig. 17. Maxwellian electron temperature axial distributions for three typical conditions

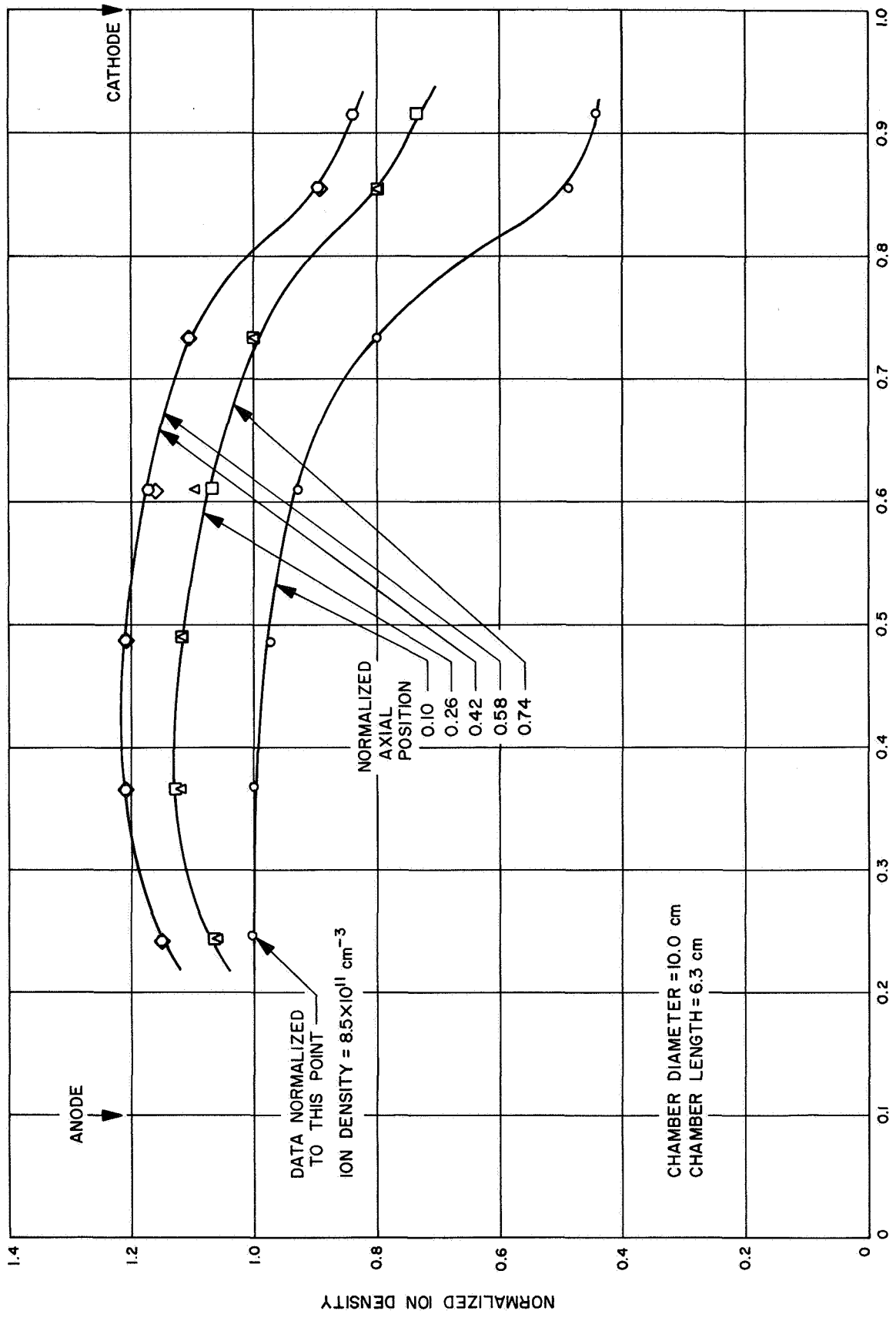

Fig. 18. Normalized ion density radial distribution for five axial locations in the reversed-current engine

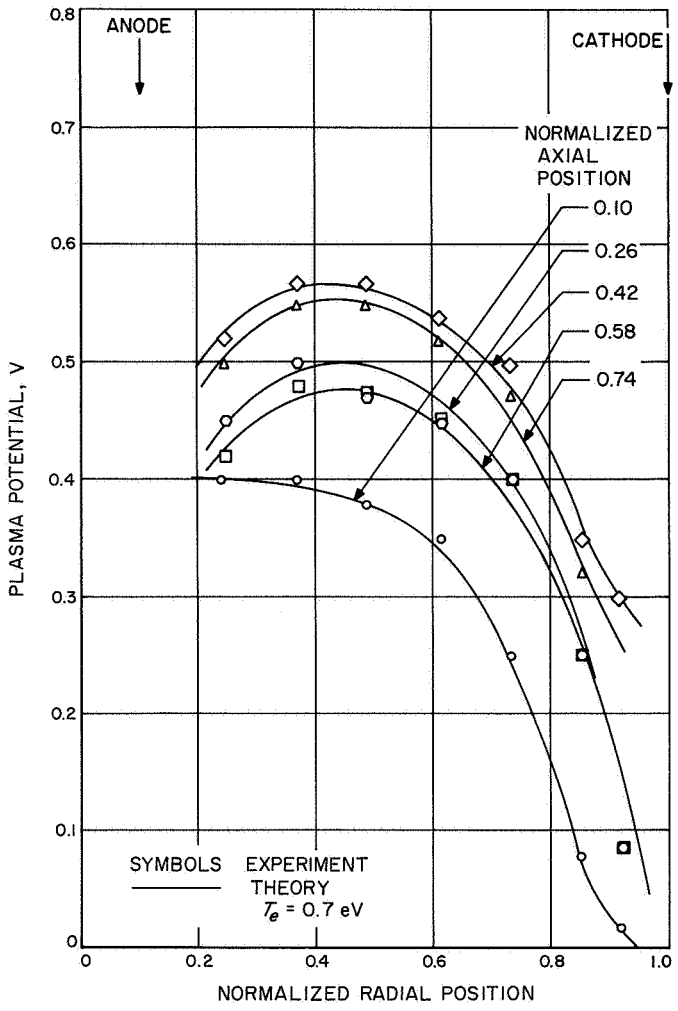

Fig. 19. Plasma potential radial distribution for five axial locations in the reversed-current engine (measured with respect to anode potential)

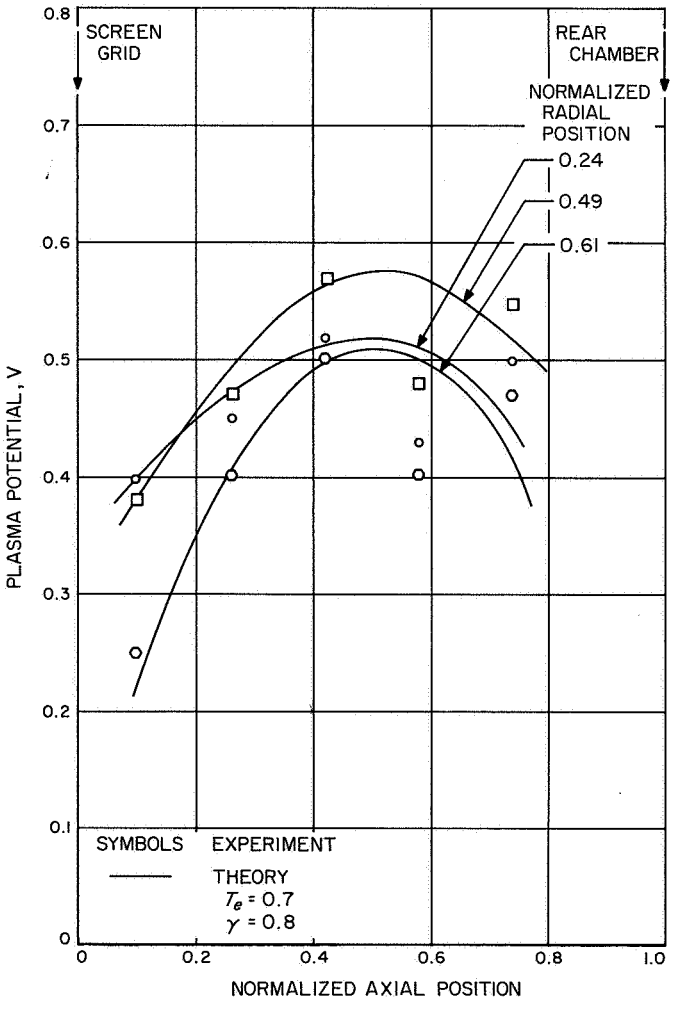

Fig. 20. Plasma potential axial distribution for three radial locations in the reversed-current engine (measured with respect to anode potential)

2. Conical engine. The measurements taken in this engine were initially reported in Ref. 18. The Maxwellian electron temperature radial distribution for one operating condition is presented in Fig. 21 for five axial positions. The corresponding ion density distribution is plotted in Fig. 22. The conditions used in the plasma potential solutions are

$$T_e = 1.5\,\text{eV} \qquad T_i/T_e = 0.05$$

$$n(0) = 4 \times 10^{11}\,\text{cm}^{-3} \qquad n_0(0) = 4 \times 10^{10}\,\text{cm}^{-3}$$

$$B = 7\,\text{G}$$

Note that, since the model assumed constant temperatures, average temperatures are used above. The radial solution simplifies to

$$\Delta V = 1.5\left[1.05 \ln\left(\frac{1 + a_3 x}{1 + a_3}\right) - \ln x\right] \qquad (75)$$

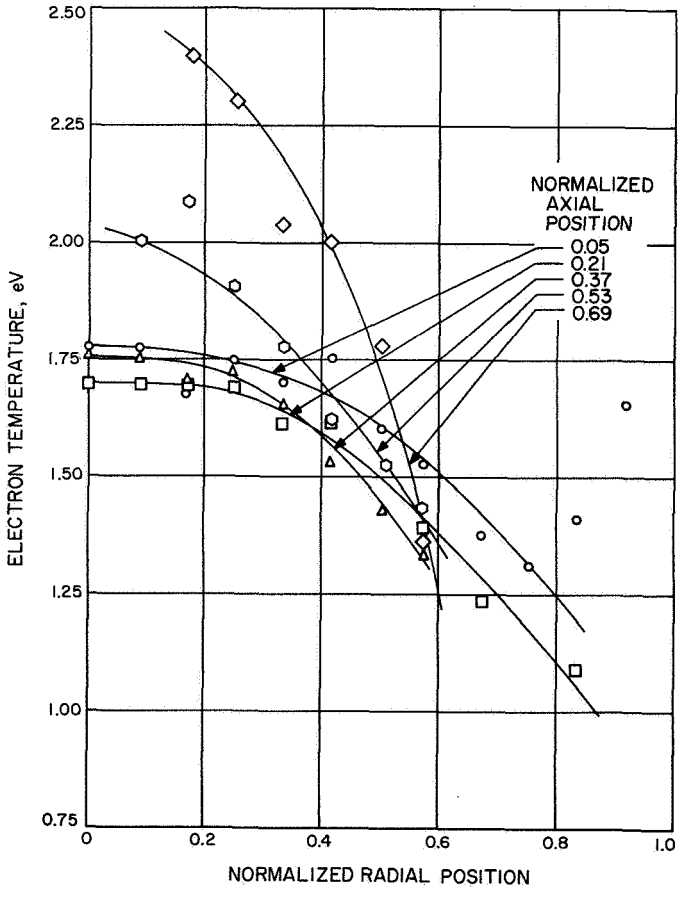

Fig. 21. Maxwellian electron temperature radial distribution for five axial locations in the conical engine

This solution fits the experimental data for a value of $\mu_i = 43\,\text{m}^2/\text{V}^{-1}/\text{s}^{-1}$, giving $a_3 = 1.33$, and is shown in Fig. 23. The axial solution reduces to

$$\Delta V = 1.5\left[1.5 \times 10^{-3}(1 - \gamma)\left(\frac{1}{x} - 1\right) - \ln x\right] \qquad (76)$$

As before, this solution is independent of γ but fits the data relatively well, as shown in Fig. 24.

C. Mercury Measurements

The engine used in the tests with mercury was previously shown schematically in Fig. 1 and is a conventional geometry type. The mercury data used in this report were also reported in Ref. 18. The measured primary and Maxwellian electron energy and temperature distributions are shown in Figs. 25 and 26, respectively, and the corresponding normalized electron density distributions in Figs. 27 and 28. In applying the model to mercury, it is necessary to neglect the primary electrons. Thus, the Maxwellian electron density and an average Maxwellian temperature are used. The conditions assumed are

$$T_e = 5.0\,\text{eV} \qquad T_i/T_e = 0.015$$

$$n(0) = 4 \times 10^{11}\,\text{cm}^{-3} \qquad n_0(0) = 4 \times 10^{10}\,\text{cm}^{-3}$$

$$B = 10\,\text{G}$$

The radial solution now becomes

$$\Delta V = 5\left[1.02 \ln\left(\frac{1 + a_3 x}{1 + a_3}\right) - \ln x\right] \qquad (77)$$

and the solution is shown fitted to the data in Fig. 29. The mobility is found to be $\mu_i = 6\,\text{m}^2/\text{V}^{-1}/\text{s}^{-1}$, and $a_3 = 1.75$. This is a rather low mobility, but it is shown that it produces approximately the measured ion current from the engine. The equation for the axial plasma potential is

$$\Delta V = 5\left[2 \times 10^{-5}(1 - \gamma)\left(\frac{1}{x} - 1\right) - \ln x\right] \qquad (78)$$

This solution is again obtained by use of the measured Maxwellian ion densities and is shown compared to the experiments in Fig. 30. Note that the validity of μ_i is not tested by the axial potential solution because of the small value of the coefficient of the term in which it appears. The solutions, Eqs. (77) and (78), are seen to agree well with the measured points. This tends to justify the neglect of primary electrons in the analysis. Further reference to neglecting the primary electrons is made in Section V.

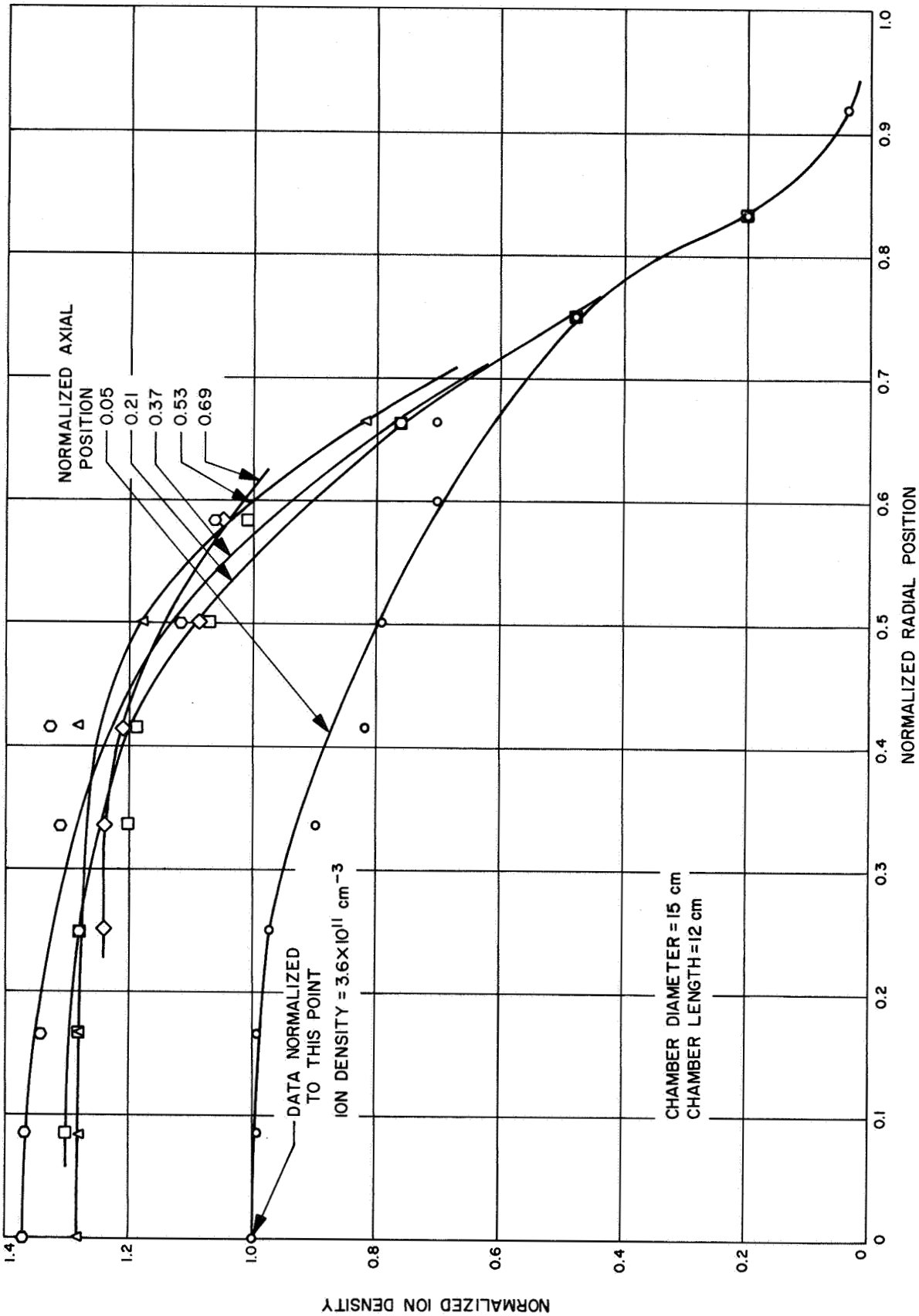

Fig. 22. Normalized ion density radial distribution for five axial locations in the conical engine

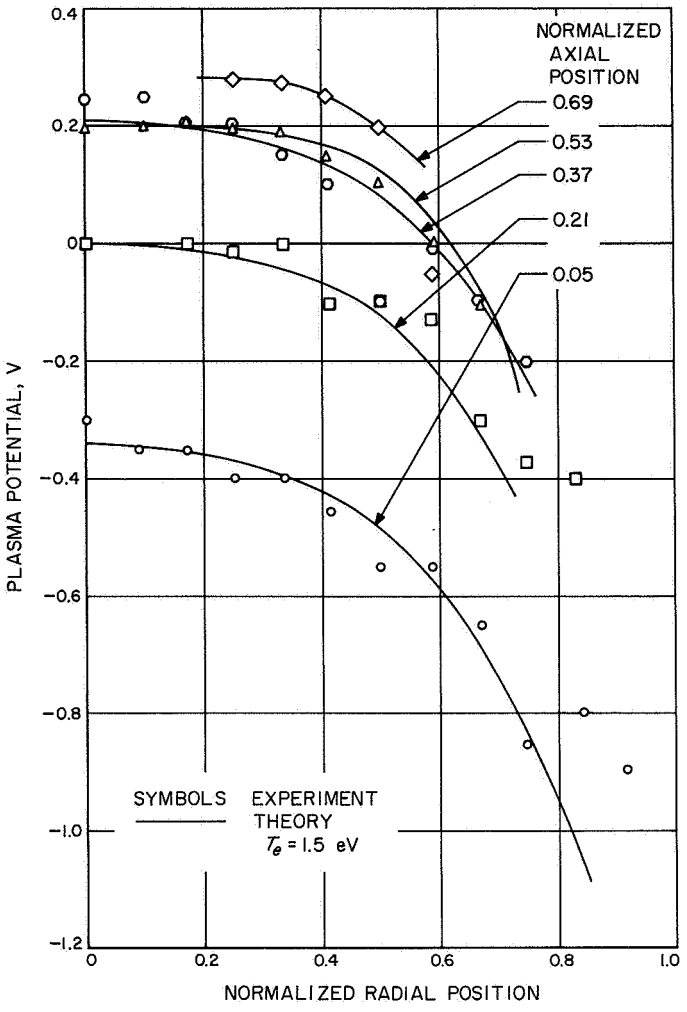

Fig. 23. Plasma potential radial distribution for five axial locations in the conical engine (measured with respect to anode potential)

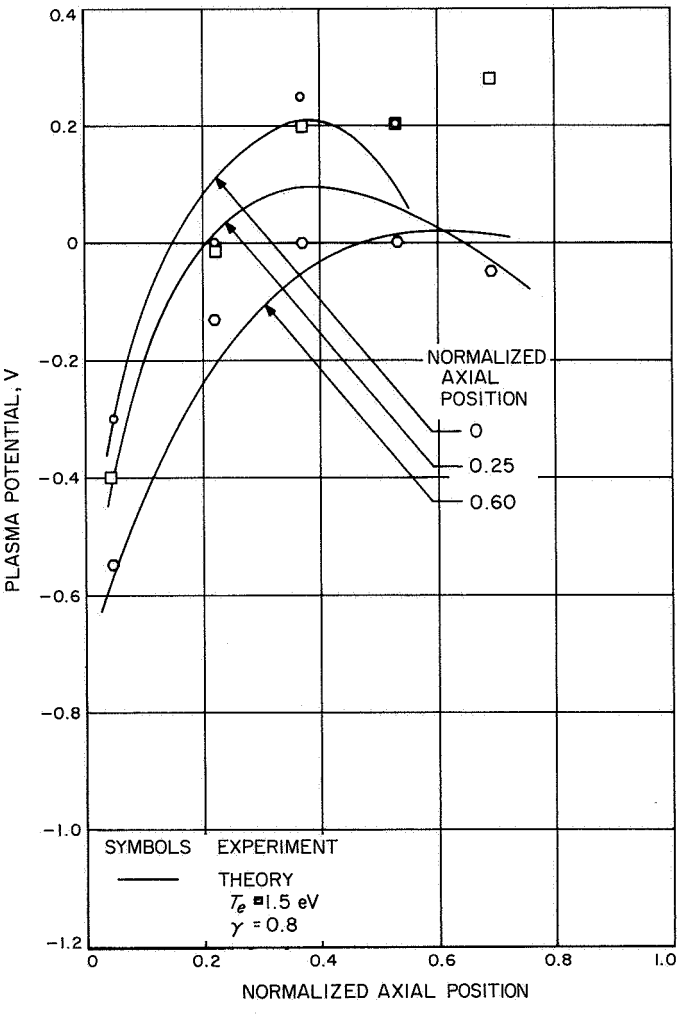

Fig. 24. Plasma potential axial distribution for three radial locations in the conical engine (measured with respect to anode potential)

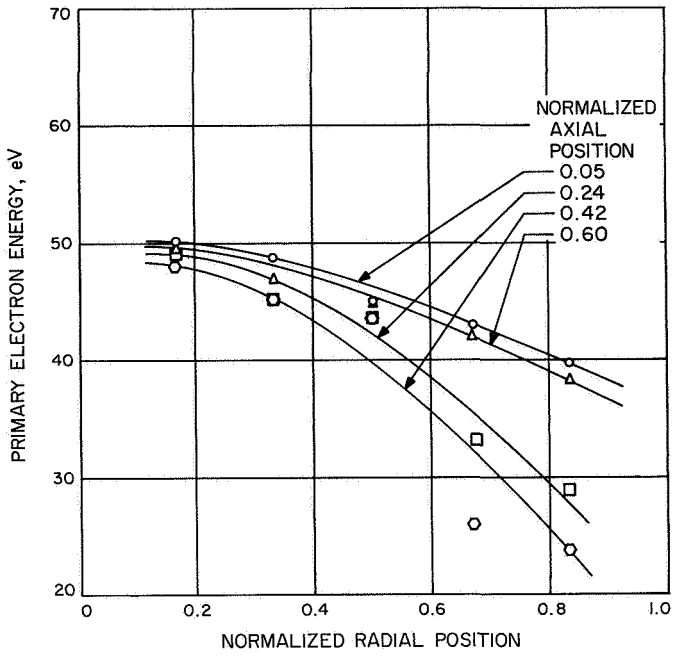

Fig. 25. Primary electron energy radial distribution for four axial locations in the mercury engine

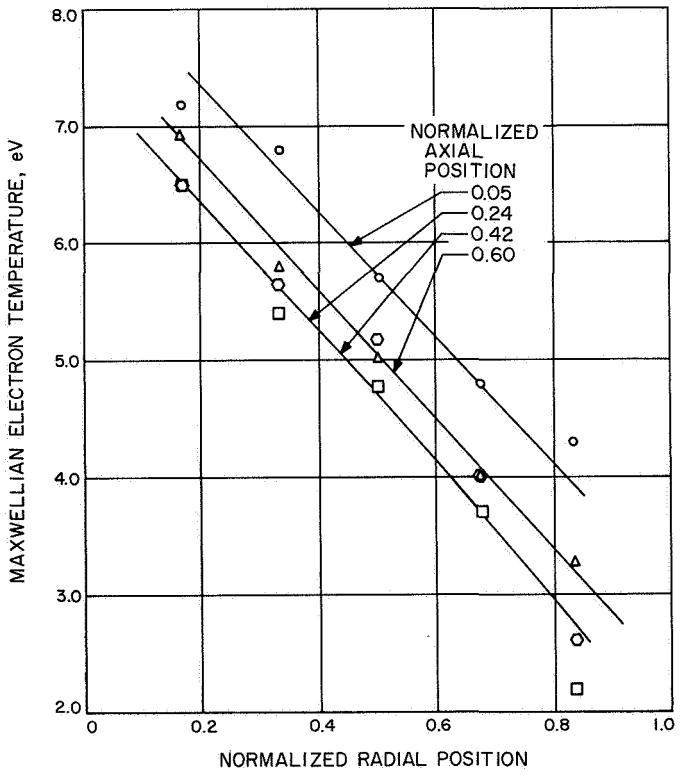

Fig. 26. Maxwellian electron energy radial distribution for four axial locations in the mercury engine

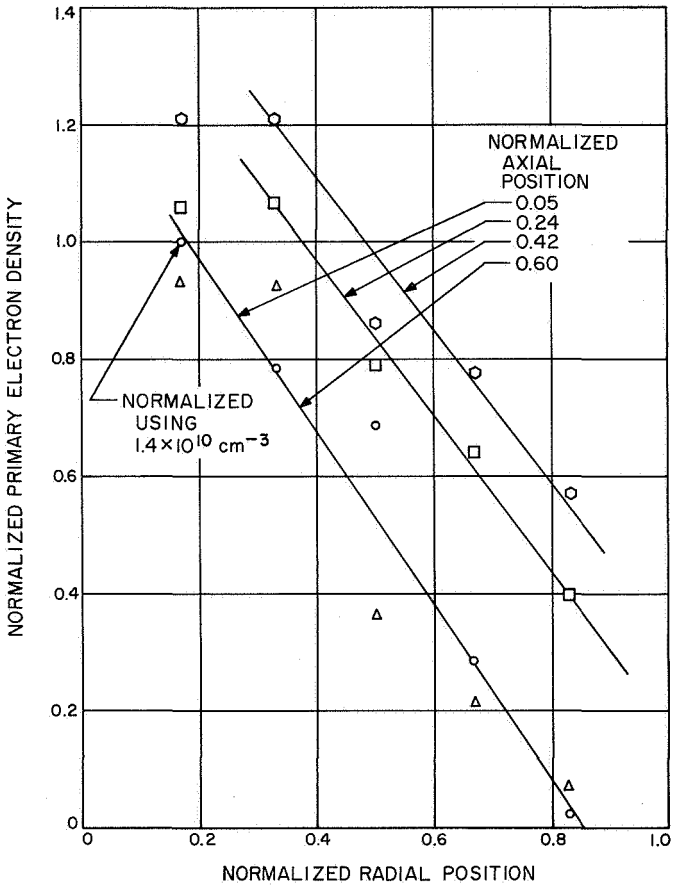

Fig. 27. Normalized primary electron density radial distribution at four axial locations

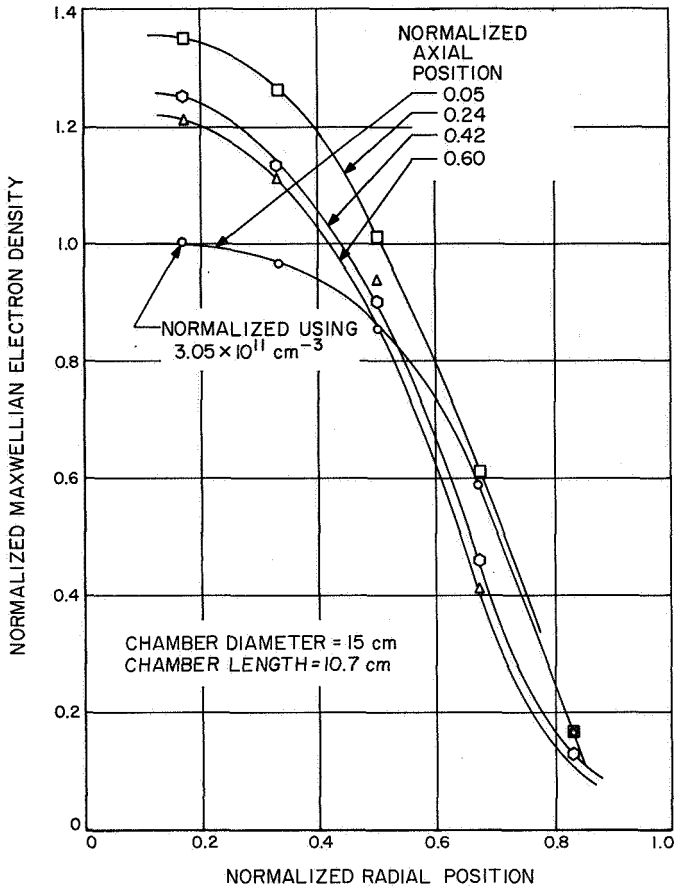

Fig. 28. Normalized Maxwellian electron density radial distribution for four axial positions in the mercury engine

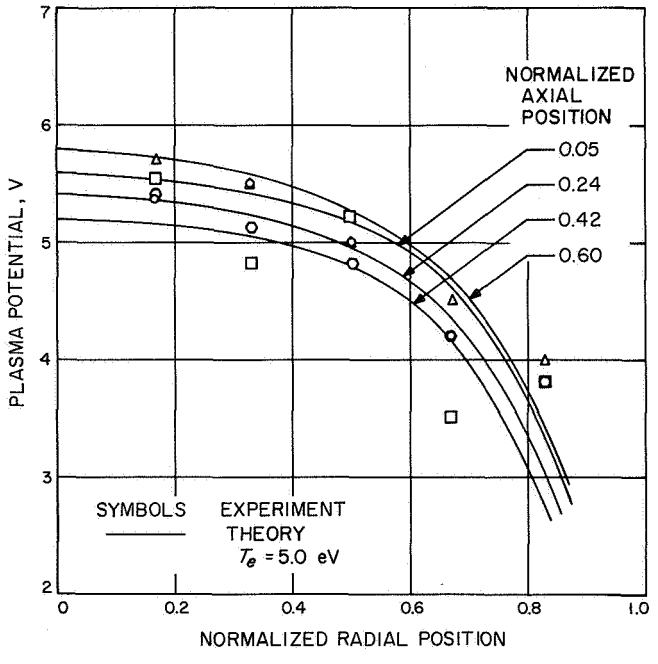

Fig. 29. Plasma potential radial distribution for four axial positions in the mercury engine (measured with respect to anode potential)

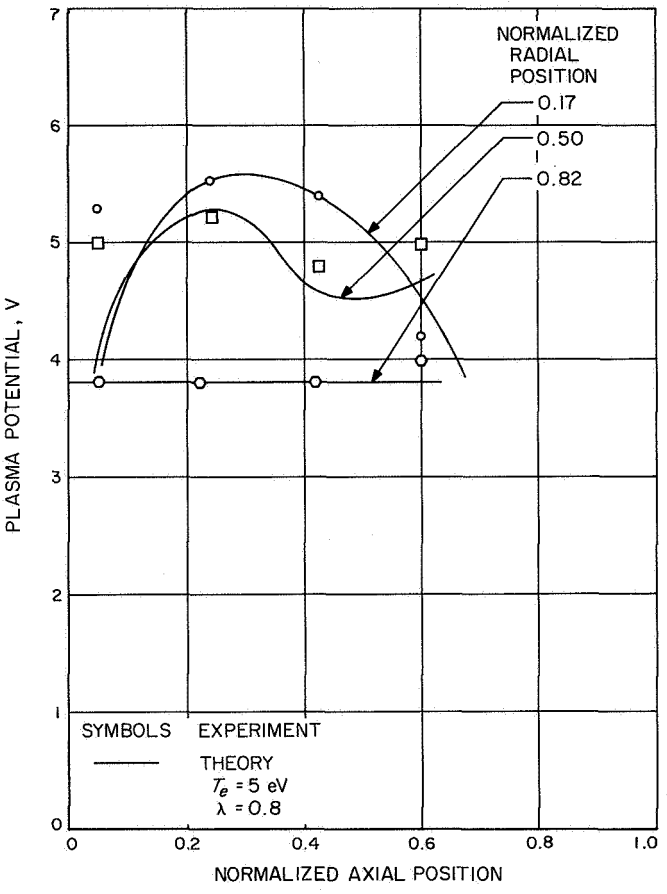

Fig. 30. Plasma potential axial distribution for three radial positions in the mercury engine (measured with respect to anode potential)

IV. Ion Beam Measurements

Ion beam current density measurements have been made with a Faraday probe using the engines described previously. Both radial and axial distributions have been measured, but only the radial distributions near the engine will be discussed here. It has been found in this work that the beam distribution changes considerably within a few inches of the engine, and thus only the measurements near the grid can be validly related to the plasma. The axial change in beam distribution has been reported in Refs. 31 and 35. A difficulty with the Faraday measurements near the engine is that the individual ion geams from each grid hole cause the data to be extremely irregular, so the beam density near the grid is approximated by fairing a curve through a plot of the maximum probe readings. The area under a curve formed in this way is greater than the measured beam current, because the ion beams leaving the engine only cover one-fourth to one-half of the grid area. Measurements taken far enough away from the engine to provide a continuous curve integrate to the correct beam current.

A typical original recording of the Faraday probe approximately 0.28 in. from the accelerating grid is shown in Fig. 31. The smooth curve is an estimate of the beam current density leaving the engine. These data were taken with the reversed-current engine, but the raggedness is typical of all the data taken near the engines. The estimated beam current densities near the accelerating grid for the three engines studied are shown in Fig. 32. The plasma conditions for these are approximately the same as those discussed previously and are close enough to allow a comparison with the model.

A comparison can now be made between the Faraday probe measurements and the ion flux predicted by Eq. (70). Using the constants presented before, and the

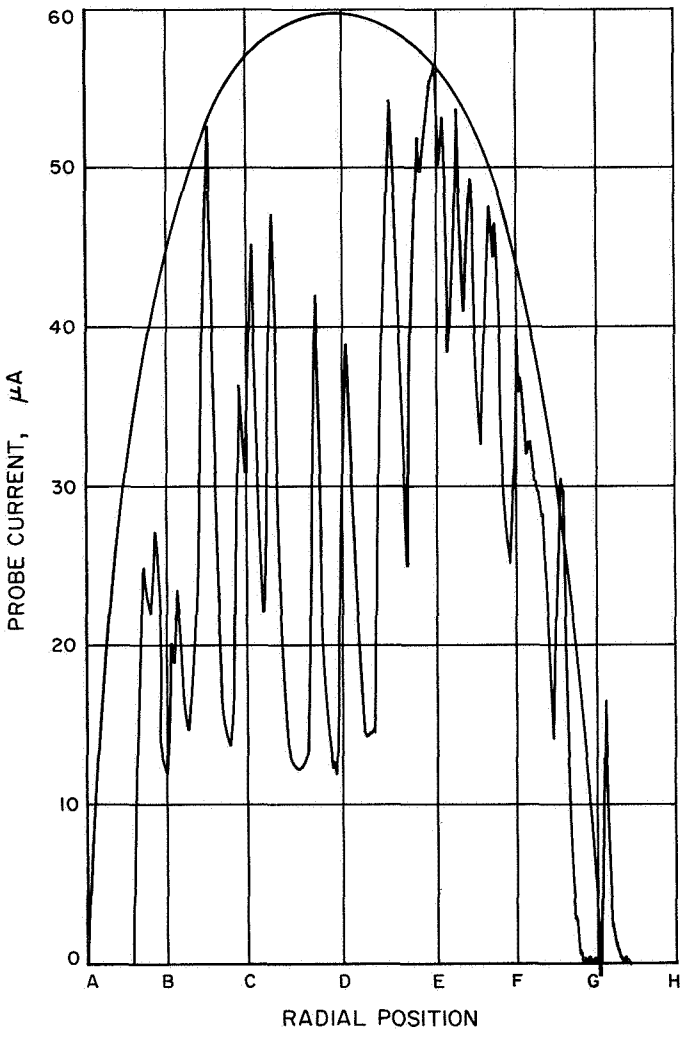

Fig. 31. Typical Faraday probe trace 0.28 in. from reversed-current engine accelerating grid

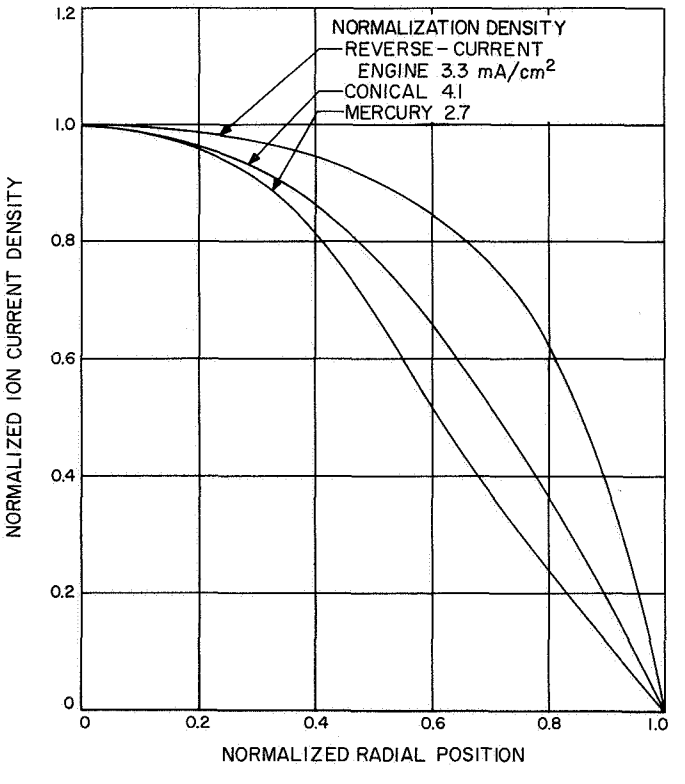

Fig. 32. Typical normalized beam current density distributions for three engines

mobility determined by the radial potential solutions, the ion flux equations at the center of the engine are:

Reverse current

$$j_i = -8.4 \times 10^{-14} \frac{\partial n}{\partial z} \tag{79}$$

Conical

$$j_i = -1.0 \times 10^{-13} \frac{\partial n}{\partial z} \tag{80}$$

Mercury

$$j_i = -4.9 \times 10^{-14} \frac{\partial n}{\partial z} \tag{81}$$

where $\partial n/\partial z$ has units of cm^{-4}. The slopes $\partial n/\partial z$ can be estimated from Figs. 18, 22, and 29, resulting in values of 5×10^{10}, 5×10^{10}, and $6 \times 10^{10}\ cm^{-4}$, respectively. When these values are used in Eqs. (79), (80), and (81), we find current densities of 4.2, 5, and 3 mA cm^{-2} for the reversed-current, conical, and mercury engines, respectively. These values agree extremely well with the typical observed current densities of Fig. 32. The agreement indicates that the model is self-consistent and that it is possible to obtain consistent values of the "effective" ion mobility by matching the model and experiment.

V. Discussion

Several of the important questions concerning the complete solution of the plasma equations can now be discussed. The assumptions, (1) neglect of primary electrons, (2) constant temperatures, (3) accounting for the ion acceleration term in the mobility, and (4) constant magnetic fields, should be assessed.

The major difficulty in solving the general plasma equations results from the primary electron group. Although this group does not appear directly in the solutions presented here, there is no guarantee that primaries do not contribute significantly to the experimental ion density through ionization. In fact, the ion production rates of Section II suggest that primaries play a large role in ionization, at least near the cathode. Since the cesium plasma is apparently free of primary electrons, a method for determining the effect of primaries is suggested. The complete solution for the ion density using the flux continuity equations could be obtained for cesium with and without ion production. If ion production throughout the plasma contributes to the ion density, primaries must be accounted for in the mercury solutions. On the other hand, if the production term does not contribute significantly to the ion distribution, the primaries could justifiably be neglected. If production in the bulk of the plasma is not important, ionization must be taking place near the cathode, with transport throughout the chamber by diffusion. The determination of the ion production process has far-reaching implications with respect to the position of the cathode, the method and position of propellant injection, and the geometrical relationship between propellant injection and the cathode.

The neglect of the ion acceleration term, with its effect included in the empirically determined mobility, is now justified by the fact that the solution works. The general numerical solutions can also be obtained using this same method by choosing mobilities which make the plasma potential ion density and axial ion flux solutions agree with measurements. This procedure should be adequate to produce closed-form solutions, since three conditions must be satisfied.

The use of average constant temperatures in the present solution is reasonable because the variation in temperature is generally much less than the variation in ion density. This allows derivatives of temperature to be neglected with respect to derivatives in density. Numerical solutions could account for temperature variations by using an assumed variation or by use of an energy equation. It would appear that average temperatures are adequate for practical purposes.

The assumption of a constant magnetic field was necessary to obtain simple analytical solutions. Numerical solutions could easily account for field variations provided the field remains axial, but additional fields would greatly complicate the equations and would couple the r, θ, and z momentum equations.

VI. Conclusions

This study has presented a framework for analyzing the plasma characteristics of the electron bombardment ion engine. A number of conclusions can be drawn from the preceding discussion and analysis:

1. A model for the electron bombardment engine has been formulated. This model accounts for all important factors in the operation of the engine. That is, it includes arc current through Γ_r^e and Γ_r^i; the magnetic field; ion production, which effectively includes the arc voltage; ion beam current; propellant distribution through the neutral density; and geometry with the proper boundary conditions.

2. Analytical solutions presented in this work indicate that much useful information could be obtained by numerically solving the plasma equations and fitting the solutions to experimental data. It is concluded in this regard that meaningful closed-form solutions could not be obtained, at least initially, without experimental data. Therefore, extrapolations through the use of assumed mobilities must be carefully considered.

3. The effect of primary electrons on the ion density must be further investigated. The method proposed to accomplish this task would also add considerable understanding to the ion production process, which is vital to the operation and efficiency of the engine. The reason the effect of primary electrons could not be determined in this study is that experimental ion densities were used and primaries did not enter into the calculations.

4. Additional probe measurements should be made, with emphasis on reducing scatter in the axial measurements. This means that all data must be obtained rather quickly in the plasma and in the beam to ensure consistent measurements.

5. The effects of magnetic field distribution, propellant feed distribution, cathode and anode position, and chamber geometry can be investigated once numerical solutions can be generalized to eliminate the fitting process. This would allow systematic engine optimization and would provide a better understanding of the electron bombardment engine.

Nomenclature

a_1, a_2, a_3 coefficients in radial plasma potential solution, Eq. (51)

A Langmuir probe area

b_1, b_2 coefficients in axial plasma potential solution, Eq. (63)

$\mathbf{B}$ magnetic field

D_i, D_e diffusion coefficient for ions and electrons

e electronic charge

$\mathbf{E}$ electric field

f electron energy distribution function

$g(\zeta)$ function in Gryzinski cross-section theory, Eq. (14)

$G(\xi)$ function in Spitzer relaxation time, Eq. (2)

i_{sm}, i_{sp} Maxwellian and primary electron current to a Langmuir probe at the plasma potential

j_i axial ion current

k Boltzmann constant

m_α mass of species α

n_α number of density of species α

N_k number of electrons in the kth state

P_α hydrostatic pressure of species α

Q collision cross section

r radial coordinate

R_m ion production function, Eq. (15)

t time

$\overline{T}_\alpha$ temperature of species α

T temperature ratio, Eq. (57)

$\mathbf{u}_\alpha$ directed velocity of species α

U_i energy for removing a single electron from the kth state

V plasma potential electron speed

V_e electron speed

x variable defined in Eq. (50)

z axial coordinate

$\delta\mathbf{u}_\alpha/\delta t$ momentum exchange term in Eq. (19)

α coefficient, Eq. (61)

β coefficient, Eq. (62)

Nomenclature (contd)

γ constant, Eq. (59)

Γ_α particle flux of species α

ϵ_α energy particles in species α

ϵ_0 permittivity of vacuum

ζ variable, Eq. (14)

η resistivity, Eq. (67)

θ azimuthal coordinate

λ function defined after Eq. (43)

Λ function defined after Eq. (1)

μ_α mobility of species α

μ mobility ratio, Eq. (55)

$\nu_{\alpha\beta}$ collision frequency between species α and β

ν_i^α production rate of species α

ν_r^α recombination rate of species α

ξ variable defined after Eq. (2)

σ function defined by Eq. (45)

Σ_α ion production coefficient for ionization by species α

τ collision times, Eqs. (1), (4), (5), (6), and (8)

$\phi(\xi)$ function defined by Eq. (3)

Subscripts

e electron

i ion

k atomic state

m Maxwellian electron

0 neutral atom

p primary electron

r, θ, z coordinates

α species

References

1. Kerrisk, D. J., "State-of-the-Art of Electric Propulsion—1965," in *AAS Science and Technology*, Vol. 6. Edited by C. M. Wong, Space Electronics Symposium, Los Angeles, Calif., 1965.

2. *Solar Powered Electric Propulsion Spacecraft Study*, Final Report, JPL Contract No. 951144. Hughes Aircraft Co., Space Systems Division, Culver City, Calif., Dec. 1965.

3. *Feasibility Study of an Ion-Propelled Mars Orbiter/Lander Spacecraft With Solar Photovoltaic Power*, Technical Report AFAPL-TR-66-109, Vols. I, II, and III. Air Force Aero Propulsion Laboratory, Research and Technology Division, Air Force Systems Command, Patterson Air Force Base, Ohio, Dec. 1966.

4. Speiser, R. C., and Branson, L. K., *Studies of a Gas Discharge Cesium Ion Source*, ARS Paper 2664-62, 17th Annual Meeting and Astronautical Exposition, Los Angeles, Calif., Nov. 12, 1962.

5. Kohlberg, I., and King, H., *Low Current Density Ion Engine Development*, Final Report, Contract NASA-1684. Ion Physics Corporation, Jan. 1963.

References (contd)

6. Strickfaden, W. B., and Geiler, K. L., "Probe Measurements of the Discharge in an Operating Electron Bombardment Engine," *AIAA J.*, Vol. 1, p. 1815, 1963.

7. Langmuir, I., and Compton, K. T., "Electrical Discharges in Gases, Part II, Fundamental Phenomena in Electrical Discharges," *Rev. Mod. Phys.*, Vol. 3, p. 191, 1931.

8. Spitzer, L., Jr., *Physics of Fully Ionized Gases.* Interscience Publishers, New York, 1962.

9. Sutton, G. W., and Sherman, A., *Engineering Magnetohydrodynamics.* McGraw-Hill Book Co., Inc., New York, 1965.

10. Sovie, R. J., and Dugan, J. V., Jr., *Energy Required for Ion Production by Electron Bombardment in Helium, Argon and Cesium,* NASA TMX-52064. National Aeronautics and Space Administration, Washington, D.C., 1964.

11. Gryzinski, M., "Classical Theory of Electronic and Ionic Inelastic Collisions," *Phys. Rev.*, Vol. 115, p. 374, 1959.

12. Arnot, F. L., and Baines, G. O., "Elastic and Inelastic Cross Sections of the Mercury Atom," *Proc. Roy. Soc.*, Vol. A151, p. 256, 1935.

13. Bleakney, W., "Probability and Critical Potentials for the Formation of Multiply Charged Ions in Mercury Vapor by Electron Impact," *Phys. Rev.*, Vol. 35, p. 139, 1930.

14. Brode, R. B., "The Quantitative Study of the Collisions of Electrons With Atoms," *Rev. Mod. Phys.*, Vol. 5, p. 257, 1933.

15. Crown, J. C., and Russek, A., "Electron–Alkali–Atom Interaction Potential Elastic-Scattering Cross Section," *Phys. Rev.*, Vol. 138, p. A669, 1965.

16. Sohl, G., Reid, G. C., Barcatta, F. A., Zafran, S., and Speiser, R. C., *Ion Rocket System Research and Development,* Final Report, NASA Contract NAS3-5250. Electro-Optical Systems, Inc., Pasadena, Calif., Dec. 1965.

17. Reader, P. D., "The Operation of an Electron Bombardment Ion Source With Various Gases," in *Electron and Ion Beam Science and Technology, 1st Inter. Conf.* Edited by R. Bakish, John Wiley and Sons, Inc., New York, 1965.

18. Masek, T. D., and Kerrisk, D. J., "Plasma Characteristics for Mercury and Cesium Bombardment Ion Engines," in *Advanced Research and Supporting Development* Space Programs Summary 37-32, Vol. IV, Jet Propulsion Laboratory, Pasadena, Calif., 1965.

19. Kerrisk, D. J., "Potentialities of Electron Bombardment Ion Engines for Electric Propulsion," *IRE Trans. Space Electron. Telemetry,* Vol. 8, p. 188, 1962.

20. Gryzinski, M., "Classical Theory of Atomic Collisions. I. Theory of Inelastic Collisions," *Phys. Rev.*, Vol. 138, p. A336, 1965.

References (contd)

21. Tate, J. T., and Smith, P. T., "Ionization Potentials and Probabilities for the Formation of Multiply Charged Ions in the Alkali Vapors and in Krypton and Argon," *Phys. Rev.*, Vol. 46, p. 773, 1934.

22. Moore, C. E., *Atomic Energy Levels*, Circular 467, Vols. I (1949), II (1952), and III (1958). National Bureau of Standards, Washington, D.C.

23. McFarland, R. H., *Gryzinski Electron Impact Ionization Cross-Section Computations for the Alkali Metals*, Report UCRL-12268. Lawrence Radiation Laboratory, Livermore, Calif., 1964.

24. Golant, V. E., "Diffusion of Charged Particles in a Plasma in a Magnetic Field," *Usp. Fiz. Nauk*, Vol. 74, p. 377, 1963; *Sov. Phys.—Usp.*, Vol. 79, p. 161, 1963.

25. Hoh, F. C., "Low-Temperature Plane Diffusion in a Magnetic Field," *Rev. Mod. Phys.*, Vol. 34, p. 267, 1962.

26. Wada, J. Y., and Knechtli, R. C., "Measurements of Electron-Ion Recombination in a Thermal Cesium Plasma," *Phys. Rev. Letters*, Vol. 10, p. 513, 1963.

27. Allis, W. P., and Buchsbaum, S. J., "Plasma Theory," in *Notes on Plasma Dynamics*, Summer Session, Vol. 1, Massachusetts Institute of Technology, Cambridge, Mass., 1959.

28. Ecker, G., "Enhanced Interaction in the Positive Column," *Phys. Fluids*, Vol. 4, p. 127, 1961.

29. Chanin, L. M., and Steen, R. D., "Mobilities of Cesium Ions in Cesium," *Phys. Rev.*, Vol. 132, p. 2554, 1963.

30. Kovar, F. R., "Mobility of Mercury Ions in Mercury Vapor," *Phys. Rev.*, Vol. 133, p. A681, 1964.

31. Kerrisk, D. J., and Masek, T. D., "Plasma Nonuniformity and Grid Erosion in an Electron Bombardment Ion Engine," *AIAA J.*, Vol. 3, p. 1060, 1965.

32. Masek, T. D., "Plasma Investigation in a Reversed Current Electron Bombardment Ion Engine," *AIAA J.*, Vol. 5, No. 4, p. 692, Apr. 1967.

33. Langmuir, I., and Mott-Smith, H. M., "Studies of Electric Discharges in Gases at Low Pressure," Parts I Through V, *G. E. Rev.*, Vol. 27, pp. 449, 583, 616, 726, and 810, 1924.

34. Mott-Smith, H. M., and Langmuir, I., "The Theory of Collectors in Gaseous Discharges," *Phys. Rev.*, Vol. 28, p. 737, 1926.

35. Sellen, J. M., Jr., Forbes, S. G., and Kemp, R. F., *Advanced Ion Beam Diagnostic Techniques*, ARS Preprint 2067-61, ARS Space Flight Report to the Nation, New York, Oct. 9–15, 1961.